

Article

Physicochemical Control of Caribbean Coral Calcification Linked to Host and Symbiont Responses to Varying $p\text{CO}_2$ and Temperature

Robert A. Eagle^{1,2,*} , Maxence Guillermic^{1,2,3} , Illian De Corte^{1,2}, Blanca Alvarez Caraveo¹, Colleen B. Bove^{4,5}, Sambuddha Misra^{6,7}, Louise P. Cameron⁸, Karl D. Castillo^{4,5} and Justin B. Ries⁸

- ¹ Department of Atmospheric and Oceanic Sciences, Institute of the Environment and Sustainability, Center for Diverse Leadership in Science, University of California, 520 Portola Plaza, Los Angeles, CA 90095, USA
 - ² Université de Brest Occidentale, Institut Universitaire Européen de la Mer, LGO, Rue Dumont d'Urville, 29280 Plouzané, France
 - ³ Department of Earth, Planetary, and Space Sciences, University of California, Los Angeles, 595 Charles Young Drive E., Los Angeles, CA 90095, USA
 - ⁴ Environment, Ecology, and Energy Program, University of North Carolina at Chapel Hill, Chapel Hill, NC 27599, USA
 - ⁵ Department of Earth, Marine, and Environmental Sciences, University of North Carolina at Chapel Hill, Chapel Hill, NC 27599, USA
 - ⁶ Indian Institute of Science, Centre for Earth Sciences, Malleshwaram, Bengaluru 560012, Karnataka, India
 - ⁷ The Godwin Laboratory for Palaeoclimate Research, Department of Earth Sciences, University of Cambridge, Cambridge CB2 3EQ, UK
 - ⁸ Department of Marine and Environmental Sciences, Marine Science Center, Northeastern University, 430 Nahant Rd, Nahant, MA 01908, USA
- * Correspondence: robeagle@g.ucla.edu



Citation: Eagle, R.A.; Guillermic, M.; De Corte, I.; Alvarez Caraveo, B.; Bove, C.B.; Misra, S.; Cameron, L.P.; Castillo, K.D.; Ries, J.B. Physicochemical Control of Caribbean Coral Calcification Linked to Host and Symbiont Responses to Varying $p\text{CO}_2$ and Temperature. *J. Mar. Sci. Eng.* **2022**, *10*, 1075. <https://doi.org/10.3390/jmse10081075>

Academic Editor: Tom Spencer

Received: 13 January 2022

Accepted: 25 July 2022

Published: 5 August 2022

Publisher's Note: MDPI stays neutral with regard to jurisdictional claims in published maps and institutional affiliations.



Copyright: © 2022 by the authors. Licensee MDPI, Basel, Switzerland. This article is an open access article distributed under the terms and conditions of the Creative Commons Attribution (CC BY) license (<https://creativecommons.org/licenses/by/4.0/>).

Abstract: It is thought that the active physiological regulation of the chemistry of a parent fluid is an important process in the biomineralization of scleractinian corals. Biological regulation of calcification fluid pH (pH_{CF}) and other carbonate chemistry parameters ($[\text{CO}_3^{2-}]_{\text{CF}}$, DIC_{CF} , and Ω_{CF}) may be challenged by CO_2 driven acidification and temperature. Here, we examine the combined influence of changing temperature and CO_2 on calcifying fluid regulation in four common Caribbean coral species—*Porites astreoides*, *Pseudodiploria strigosa*, *Undaria tenuifolia*, and *Siderastrea siderea*. We utilize skeletal boron geochemistry (B/Ca and $\delta^{11}\text{B}$) to probe the pH_{CF} , $[\text{CO}_3^{2-}]_{\text{CF}}$, and DIC_{CF} regulation in these corals, and $\delta^{13}\text{C}$ to track changes in the sources of carbon for calcification. Temperature was found to not influence pH_{CF} regulation across all $p\text{CO}_2$ treatments in these corals, in contrast to recent studies on Indo-Pacific pocilloporid corals. We find that $[\text{DIC}]_{\text{CF}}$ is significantly lower at higher temperatures in all the corals, and that the higher temperature was associated with depletion of host energy reserves, suggesting $[\text{DIC}]_{\text{CF}}$ reductions may result from reduced input of respired CO_2 to the DIC pool for calcification. In addition, $\delta^{13}\text{C}$ data suggest that under high temperature and CO_2 conditions, algal symbiont photosynthesis continues to influence the calcification pool and is associated with low $[\text{DIC}]_{\text{CF}}$ in *P. strigosa* and *P. astreoides*. In *P. astreoides* this effect is also associated with an increase in chlorophyll a concentration in coral tissues at higher temperatures. These observations collectively support the assertion that physicochemical control over coral calcifying fluid chemistry is coupled to host and symbiont physiological responses to environmental change, and reveals interspecific differences in the extent and nature of this coupling.

Keywords: Caribbean; coral; calcification; pH regulation; boron isotopes; B/Ca; carbon isotopes; photosynthesis; bleaching; symbiont

1. Introduction

Corals are foundational for some of earth's most biologically productive and diverse ecosystems, many of which are threatened by a combination of rising ocean temperatures, disease, ocean acidification (OA), and other pressures. Ocean warming can cause a breakdown in the symbiotic relationship between corals and their algal symbionts leading to coral "bleaching" and eventual mortality [1] and represents a significant threat to corals [2]. In addition, as atmospheric carbon dioxide partial pressure continues to rise, so does uptake of CO₂ into seawater, which reduces seawater pH (pH_{SW}) and calcium carbonate saturation state (Ω), thereby making seawater less chemically favorable for organisms that produce CaCO₃ shells and skeletons [3]. However, it is understood that some species of marine calcifying organisms are resilient to external acidification or may even benefit by utilizing the additional dissolved inorganic carbon (DIC) available for shell building, and in some cases photosynthesis [4–7].

Coral calcification responses to ocean acidification are known to be diverse, with observations of negative skeletal growth responses [8–20]. Coupled ocean acidification and temperature stress has revealed a variety of responses due to interactions with temperature stress, including negative synergistic [14,21–24].

Whilst interactive effects of temperature and acidification on corals are known, the underlying physiological causes of those effects are less well understood. In two Indo-Pacific pocilloporid coral species, *Pocillopora damicornis* and *Stylophora pistillata*, we observed that corals cultured at 28 °C exhibit increased net calcification with increasing pCO₂, but a shift to negligible or negative net calcification at 31 °C [7]. At the 28 °C treatment, CO₂ fertilization of symbiont photosynthesis appeared to be occurring, which supplied the energy resources for corals to increase calcification [7,25]. At 31 °C, loss of symbiont density was observed from coral color analyses [7,25]. Using two independent approaches, pH microelectrodes and skeletal boron geochemistry, it was found that temperature compromised the corals' ability to maintain biological regulation of its internal parent fluids for calcification (calcifying fluids; CF), with pH_{CF} and [CO₃²⁻]_{CF} reduced at 31 °C and more sensitive to changes in the carbonate chemistry of external seawater [7]. Similar observations using pH sensitive dyes [26] and geochemical proxies [27–29] have been reported in field-collected corals with different thermal exposure histories. As it is thought that biological upregulation of the pH_{CF}, [CO₃²⁻]_{CF}, [DIC]_{CF}, and the saturation state of aragonite (Ω_{Ar})_{CF} is important in allowing corals to calcify [30–35], loss of this control on thermal stress may explain how temperature and pCO₂-induced ocean acidification could interact to negatively impact coral calcification [7]. Both laboratory experiments and observations on field collected corals have their limitations. In culture experiments, the question is how well are natural physiological responses to stressors simulated by the experiment and, in field collected corals, it can be difficult to constrain and disentangle complex and covarying relationships between the seawater carbonate system and their geochemical proxies [36]. Whilst coral calcifying chemistry regulation in response to acidification has been widely investigated in Indo-Pacific species, it has not to our knowledge been examined in depth in culture experiments on the Caribbean species studied here, with the exception of a study by [37] on *S. siderea* using a spatially resolved laser ablation approach.

Here, we further explore the independent and combined effect of temperature and pCO₂ on coral and algal symbiont physiology in a study on four species of common Caribbean scleractinian corals *Porites astreoides*, *Pseudodiploria strigosa*, *Undaria tenuifolia*, and *Siderastrea siderea* (Figure 1). These corals were recovered from the Belize Mesoamerican Barrier Reef System, cultured at 28 °C and 31 °C, and at ~280 to 3300 μ atm pCO₂, and characterized for their structural and physiological responses to these conditions [38,39]. The coral species exhibited interspecific variations in host and symbiont responses to changing environmental conditions in the experiment, which allows us to investigate the link between host and symbiont physiology and the control of calcification and calcification fluid chemistry [38,39]. It was found that all four coral species exhibited nonlinear decreases in net calcification rate with increasing pCO₂ [38]. The 31 °C treatment reduced calcification

rate in only one species, *P. strigosa*, although *U. tenuifolia* exhibited too low survival rates at 31 °C to be assessed [38]. *Siderastrea siderea* was the most resilient coral maintaining positive rates of net calcification under all conditions, even when seawater was undersaturated with respect to aragonite [38]. *Siderastrea siderea* was found to maintain relatively unaltered symbiosis under experimental conditions, and relatively constant host energy reserves, consistent with its resilient calcification response [39]. *Pseudodiploria strigosa* did not maintain indicators of coral symbiont physiology under warming, such as chlorophyll content and symbiont cell density, and was the most bleached coral in the experiment [39]. Conversely, *P. astreoides* exhibited improved symbiont physiological indicators and chlorophyll content at 31 °C, which were reduced under the acidification conditions [39], although the 31 °C condition was characterized by lower survival rates [38]. *Pseudodiploria strigosa* and *S. siderea* showed stronger correlations between symbiont density and host energy reserves, consistent with a tighter coupling between these physiological indicators than were found in *P. astreoides* [39]. It was concluded in previous work that this may result from *P. astreoides* symbionts being more efficient in delivering autotrophically derived carbon to the host, whereas *P. strigosa* and *S. siderea* require relatively greater concentrations of their symbionts to support the host [39]. Therefore, this experiment represents an opportunity to expand on our previous work [7] to explore the underlying mechanisms behind the interaction of temperature and $p\text{CO}_2$ on corals and, in particular, how symbiont and host physiological responses could influence corals' ability to exert active biological control on physicochemical parameters, such as pH_{CF} , $[\text{DIC}]_{\text{CF}}$, and $[\text{CO}_3^{2-}]_{\text{CF}}$. We applied a combined approach of boron geochemistry to constrain pH_{CF} , $[\text{DIC}]_{\text{CF}}$, and $[\text{CO}_3^{2-}]_{\text{CF}}$ and $\delta^{13}\text{C}$ to trace changes in the source of carbon for calcification linked to coral and symbiont physiological responses to environmental changes.

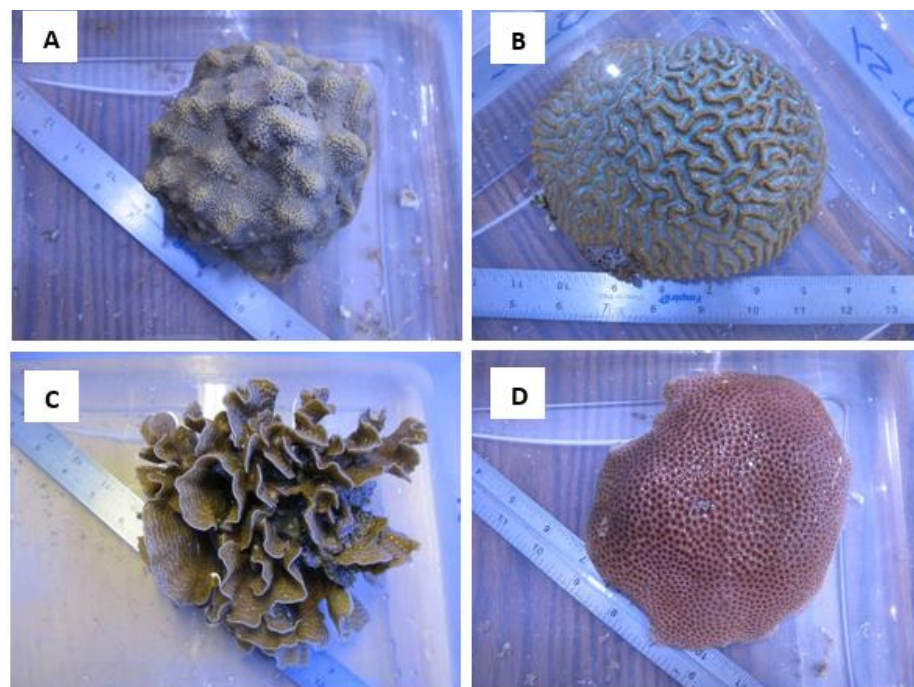


Figure 1. Sample photographs of the coral species cultured in the experiment of Bove et al. (2019) [38] and investigated here: (A) *Porites astreoides*, (B) *Pseudodiploria strigosa*, (C) *Undaria tenuifolia*, and (D) *Siderastrea siderea*.

2. Materials and Methods

2.1. Sample Collection

Samples from the tropical Caribbean Scleractinian coral species *Siderastrea siderea*, *Pseudodiploria strigosa*, *Porites astreoides*, and *Undaria tenuifolia* (Figure 1) were collected from inshore and offshore reef environments along the southern portion of the Mesoamerican

Barrier Reef System (MBRS) off the coast of Belize in June 2015, at depths of 3–5 m [38]. For each species, six colonies were collected from both an inshore and offshore reef environment, totaling 48 colonies (4 species \times 6 colonies \times 2 reef environments), as described in Supplementary Table S3. Samples were then transported to a natural seawater flow-through aquarium system at Northeastern University's Marine Science Center in Nahant, MA, USA, where each colony was sectioned into eight fragments to be acclimated and subsequently undergo the 93-day experiment [38]. New data from a second experiment on Indo-Pacific corals are also presented here, in this experiment specimens of *Stylophora pistillata*, were obtained from DeJong MarineLife (Lingewaal, The Netherlands) and cultured as described previously [7,25].

2.2. Experimental Culturing

Following a ~70 day conditioning period, fragmented coral colonies from *S. siderea*, *P. strigosa*, *P. astreoides*, and *U. tenuifolia* were reared for 93 days under four $p\text{CO}_2$ conditions corresponding to preindustrial (311 μatm), present-day control (405 μatm), end-of-century (701 μatm), and extreme (3309 μatm) carbon dioxide partial pressures, and under two temperature conditions corresponding to control (28 °C, as determined by in situ reef temperature records near the collection site) and elevated temperature treatments (31 °C), as predicted for end-of-century mean sea-surface temperature near the collection site [40]. The extreme $p\text{CO}_2$ condition allows for an exploration of the physiological limits of the species, as well as simulates conditions in past greenhouse periods in earth history which are relevant to understand coral evolution. Coral fragments within each tank were fed every other day with a mixture of ca. 6 g frozen adult *Artemia* sp. and 250 mL concentrated newly hatched live *Artemia* sp. (500 mL^{-1}) to satisfy any heterotrophic feeding by each species. Supplementary Tables S1 and S2 reproduce the measured and calculated experimental parameters from the original study [38].

2.3. Net Calcification Rate, Coral Symbiont and Host Physiological Measurements

Net coral calcification rates from this experiment were estimated from surviving coral fragments using the buoyant weight method, as described in [38], and reported in units of $\text{mg cm}^{-2} \text{d}^{-1}$. Algal symbiont cell density was assessed using Lugol's iodine staining, with cell counts standardized to total coral tissue volume to yield values in cells per cm^2 as described in [39]. Chlorophyll a (Chl a) was measured on a Turner Design 10-AU fluorometer and expressed in units of g of pigment per cm^2 of coral tissue surface area [39]. Coral host protein, host lipids, and host carbohydrate were determined by spectrophotometry and recorded in units of mg per cm^2 of coral tissue surface area. Whilst these data have been reported in previous publications [38,39], they are reproduced here in Table S3 to provide easy reference for interpreting the geochemical data.

2.4. Coral Sample Preparation for Geochemical Analyses

New skeletal growth was identified relative to a calcein marker emplaced in the coral skeleton at the start of the experiment, which was visualized using fluorescent light microscopy [38]. Powdered and homogenized samples underwent clay-removal and oxidative cleaning following the method from Barker et al. [41]. Sample material was then dissolved in 1 M HCl (80–100 μL).

2.5. Boron Isotopic Analysis

Boron was purified via microdistillation [42,43] following similar methods described in our previous work [7,44]. Measurements were carried out on a Thermo Scientific® Neptune Plus MC-ICP-MS at the University of Cambridge equipped with $10^{13} \Omega$ resistors [45]. Boron isotopic composition is reported in standard $\delta^{11}\text{B}$ per mil (‰) notation with respect to the NIST SRM 951a boric acid standard (Catanzaro et al., 1970). A laboratory coral standard (NEP; *Porites* sp.) from the University of Western Australia and the Australian National

University was analyzed for assessing internal reproducibility between analytical sessions as well as external reproducibility with other labs.

Sample blanks typically contained less than 0.6 ng-B (<5 ppb B). The $\delta^{11}\text{B}$ composition of the NEP ($\delta^{11}\text{B}_{\text{NEP}}$) was measured at $25.6 \pm 1.0\%$ (2 SD, $n = 20$) across 13 analytical sessions (Table S4), with each number representing an ab initio processed sample from the present study, which are within analytical uncertainty of published values for the same in-house standard of $25.96 \pm 0.30\%$, $26.2 \pm 0.88\%$, $n = 27$, ($25.8 \pm 0.89\%$, $n = 6$, $25.71 \pm 0.79\%$, $n = 27$, from [46–48]). The proposed international standard JCP–1 [49] was not analyzed across our analytical sessions due to lack of availability, nevertheless, previous work [7,44] was performed over the same period and report values within analytical uncertainty of published data, thereby validating the method utilized in the present study [7,49].

2.6. B/Ca Analysis

Elemental ratios were analyzed on a Thermo Scientific® Element HR ICP-MS at Cambridge University, UK and at European Institute for Marine Studies (IUEM), France, after calcium concentration checks on the Agilent® ICP-OES at Cambridge University, UK and at IUEM, France. Isotope concentrations of the acid blanks relative to a typical Ca concentration session (10 ppm) were: $\text{Li}^7 < 7\%$, $\text{B}^{11} < 0.75\%$, $\text{Mg}^{25} < 0.5\%$, $\text{Sr}^{87} < 0.01\%$, $\text{Ca}^{43} < 0.1\%$. External reproducibility is reported relative to the consistency standard CamWuellestorfi, as published by [43] and measurements of the NEP coral. Our data were within one standard error of published values (Table S5). The analytical uncertainties (2sd) on the B/Ca ratios were 15 $\mu\text{mol/mol}$.

2.7. Modelled pH_{CF}

The pH of the calcifying fluid (pH_{CF}) was calculated from the boron isotopic composition of the coral skeleton following rationale from Hemming and Hanson [50] and using the MATLAB code provided in De Carlo et al. [51], where $\delta^{11}\text{B}_{\text{SW}}$ represents the boron isotopic composition of seawater ($\delta^{11}\text{B}_{\text{SW}} = 39.61\%$) [52] and $\delta^{11}\text{B}_{\text{CARB}}$ represents the boron isotopic composition of the coral skeleton. The isotopic fractionation factor between the boron forms from Klochko et al. (2006) was used, $\alpha_{(\text{B3-B4})} = 1.0272$. The dissociation constant of boron (K_{B}) was calculated from salinity, temperature and pressure [53], and the boron concentration was calculated from salinity after Lee et al., 2010 [54].

$$\text{pH}_{\text{CF}} = \text{p}K_{\text{B}} - \log\{-[\delta^{11}\text{B}_{\text{SW}} - \delta^{11}\text{B}_{\text{CARB}}]/[\delta^{11}\text{B}_{\text{SW}} - \alpha_{(\text{B3-B4})} * \delta^{11}\text{B}_{\text{CARB}} - \varepsilon_{(\text{B3-B4})}]\} \quad (1)$$

$[\text{H}^+]_{\text{SW}}$ and $[\text{H}^+]_{\text{CF}}$ were calculated based on pH_{SW} and pH_{CF} with $[\text{H}^+] = 10^{-\text{pH}}$. The proton gradient $[\text{H}^+]_{\text{SW}} - [\text{H}^+]_{\text{CF}}$ was evaluated to better visualize the scale of pH regulation in comparison to a logarithmic scale.

2.8. Modelled $[\text{CO}_3^{2-}]_{\text{CF}}$, DIC_{CF} , and Ω_{CF}

DIC_{CF} and $[\text{CO}_3^{2-}]_{\text{CF}}$ were calculated using the method and Matlab® code from DeCarlo et al. [51]. This study uses combined B/Ca and $\delta^{11}\text{B}$ to calculate $[\text{CO}_3^{2-}]_{\text{CF}}$, where:

$$[\text{CO}_3^{2-}]_{\text{CF}} = K_{\text{D}} * \frac{[\text{B}(\text{OH})_4^-]}{\text{B/Ca}} \quad (2)$$

We use the K_{D} defined in McCulloch et al. [33], $K_{\text{D}} = 0.00297 * \exp(-0.0202 * [\text{H}^+])$, where $[\text{H}^+]$ is determined based on pH_{CF} as calculated from $\delta^{11}\text{B}$ following Equation (1). Given pH_{CF} and $[\text{CO}_3^{2-}]_{\text{CF}}$, DIC_{CF} can be calculated using the known dissociation constants for carbonate speciation at known temperatures and pressure. Ω_{CF} can also be calculated but requires an additional assumption on the $[\text{Ca}^{2+}]$ of the calcifying fluid. The saturation state of aragonite in the calcifying medium (Ω_{CF}) defined following Equation (3)

is dependent on the accuracy of the $[\text{CO}_3^{2-}]_{\text{CF}}$ and is limited to the additional assumption on the $[\text{Ca}^{2+}]$ of the calcifying fluid.

$$[\Omega]_{\text{CF}} = \frac{[\text{CO}_3^{2-}]_{\text{CF}} \times [\text{Ca}^{2+}]_{\text{CF}}}{K_{\text{sp}}} \quad (3)$$

We calculated the saturation state of aragonite of the calcifying fluid using the $[\text{Ca}^{2+}]_{\text{sw}}$ determined using the salinity of the culture condition ($[\text{Ca}^{2+}]_{\text{sw}}$ (mol/kg sw) = $0.02128/40.1 \times (\text{Salinity} - 0.03)/1.805$).

2.9. Carbon Stable Isotope Analyses

Analyses on Caribbean corals were conducted on two Nu Perspective isotope ratio mass spectrometers (IRMS) at UCLA [55]. Most samples were analyzed using a Nu Carb specific sample preparation system. This system reacts 0.48 mg (± 0.03 mg) of pure calcium carbonate material, for 20 min at 70 °C in individual reaction vials, thus eliminating any potential memory effects that are associated with analyses using a common acid bath system. Gases released by acid digestion of CaCO_3 are purified in a series of liquid N₂-cooled, temperature controlled cold-fingers, an Adsorption Trap (AdTrap), an in-line, short Gas Chromatograph (GC) column packed with Porapak Type-QTM50/80 and silver wool, before introduction to the mass-spectrometer dual inlet for isotope analysis. The second digestion system is the common acid bath (CAB) system [55]. Analyses of *Stylophera pistillata* skeletal $\delta^{13}\text{C}$ and $\delta^{18}\text{O}$ was carried out on a GasBench II coupled to a Delta V mass spectrometer at the stable isotope facility of Pôle spectrometrie Océan (PSO), Plouzané, France. Results were calibrated to the Vienna Pee Dee Belemnite (V-PDB) scale and referenced to the international standard NBS19.

2.10. Statistical Methods

For elemental data, the most restrictive false discovery rate ($Q = 0.1\%$) was used to thin data using the ROUT method set, meaning that $<0.1\%$ of identified outliers would have been falsely identified as such. To test for statistically significant changes in net calcification, we performed a one-way ANOVA followed by Dunnett's multiple comparisons tests on skeletal B/Ca composition, $\delta^{11}\text{B}$, $\delta^{13}\text{C}$, pH_{CF} , and Ω_{CF} across experimental treatment conditions relative to the control condition (28 °C, 400 μatm pCO_2). To determine the best fit by linear or second-order polynomial (quadratic) regressions, we used a combined linear and quadratic fit test, using the Akaike's Information Criteria (AIC). We compared the best-fit regressions across temperature conditions by first determining if the slopes of the two regressions are statistically different, and if the slopes are not significantly different (p -value > 0.05), we tested to see if the intercepts were significantly different (p -value < 0.05). This was done using an Analysis of Covariance (ANCOVA) method. The statistical analyses above were carried out GraphPad Prism version 9.0.0 for macOS, GraphPad Software, San Diego, CA, USA.

$\delta^{11}\text{B}$, B/Ca, and $\delta^{13}\text{C}$ data were tested to see if it met assumptions of normality using the Shapiro–Wilks test ($p > 0.05$). At the level $p < 0.05$ we found that most of the data were not normally distributed. In order to perform a two-way ANOVA test, we transformed the data using the Tukey ladder of powers method to reduce negative and positive skew of non-normal data methodologically [56]. Method until it met the test of normality. Table S6 gives information about whether data were transformed and how they were transformed. Following confirmation that the data were normal, we analyzed isotope and elemental data using a two-way ANOVA to test the influence of the individual and combined effects of pCO_2 and temperature. The same approach was taken to analyze the calculated parameters pH_{CF} , $[\text{CO}_3^{2-}]_{\text{CF}}$, and DIC_{CF} and the coral and symbiont physiological data; calcification rate, symbiont cell density, chlorophyll a, and total host energy data from [38,39]. All statistical analysis was conducted using the 'MASS' package in R version 4.0.2 (R Core Development Team 2016, Vienna, Austria).

As coral species were collected from inshore and offshore reef environments, so we also tested whether there were significant effects of temperature, $p\text{CO}_2$, and reef environment on geochemical and physiological parameters in a three-way ANOVA. As this analysis did not resolve a significant effect of reef environments, it justified the pooling of data across reef environments to conduct the two-way ANOVA tests described above.

2.11. Data Compilation

Data from previous publications was compiled to construct synthesis figures on coral calcifying fluid chemistry derived from geochemistry and other approaches such as electrodes and pH sensitive dyes. Literature data used for this metanalysis is summarized in Table S12 and was derived from the following publications [7,17,32,34,35,47,57–70]. In order to include the data from Allison et al., 2014 [32] on the carbonate chemistry of the calcification fluid from *P. damicornis* cultured under different concentrations of the ruthenium red (RR, 3.7 and 5.3 μM) inhibitor of Ca-ATPase activity, new calculations of the original data were performed using the framework described in this paper. Carbonate chemistry of the cultured experiments were calculated from alkalinity and pH provided in a previous publication [71] and using the CO_2sys program [72].

3. Results

3.1. Analyses of ($\delta^{11}\text{B}$), B/Ca, and $\delta^{13}\text{C}$

Mean boron geochemistry ($\delta^{11}\text{B}$ and B/Ca) and $\delta^{13}\text{C}$ for each experimental condition of the Caribbean coral experiment are reported in Table 1, individual coral specimen data are reported in Table S7. B/Ca ($\pm\text{SD}$) measurements for the control culturing conditions were averaged for each species under the experimental control conditions of 28 °C and 405 $\mu\text{atm } p\text{CO}_2$: *P. astreoides* ($437 \pm 31 \mu\text{mol/mol}$), *P. strigosa* ($495 \pm 70 \mu\text{mol/mol}$), *S. siderea* ($436 \pm 18 \mu\text{mol/mol}$), *U. tenuifolia* ($518 \pm 32 \mu\text{mol/mol}$). Under the experimental control culturing conditions, coral skeletal aragonite $\delta^{11}\text{B}$ compositions ($\pm\text{SD}$) were averaged for each species: *P. astreoides* ($24.54 \pm 0.74\text{‰}$), *P. strigosa* ($24.40 \pm 1.40\text{‰}$), *U. tenuifolia* ($24.63 \pm 0.68\text{‰}$), and *S. siderea* ($23.87 \pm 0.47\text{‰}$). Mean $\delta^{13}\text{C}$ ($\pm\text{SD}$) for each species under the control temperature and $p\text{CO}_2$ experimental condition (28 °C, 405 $\mu\text{atm } p\text{CO}_2$) was: *P. astreoides* ($-2.58 \pm 0.92\text{‰}$), *P. strigosa* ($-1.11 \pm 1.51\text{‰}$), *S. siderea* ($-3.94 \pm 0.61\text{‰}$), and *U. tenuifolia* ($-2.65 \pm 0.34\text{‰}$) (Table 1).

Boron geochemical data for *S. pistillata* have previously been reported in Guillermic et al. Here, we report $\delta^{13}\text{C}$ and $\delta^{18}\text{O}$ data from *S. pistillata* skeletal aragonite from this additional experiment on Indo-Pacific corals, given in Table S8. The principal reason for presenting these data in this study is that they provide context for the interpretation of data from the Caribbean corals, as described in more detail below.

Trends in measured geochemical parameters as a function of culture seawater pH (pH_{SW}) were explored using Akaike's Information Criteria (AIC) to determine whether a linear or second-order polynomial (quadratic) regression best fit the data (Figure 2; Table S9). In all cases, a linear regression was found to fit the data better, with the exception of $\delta^{11}\text{B}$ and B/Ca data for *S. siderea*, where a nonlinear fit was preferred (Figure 2, Table S9). In terms of geochemical proxy development for historical seawater pH reconstruction, the three species that exhibited relationships between $\delta^{11}\text{B}$ and pH_{SW} that were best described by linear regressions seem best suited for this endeavor. *P. strigosa* showing the greatest sensitivity of $\delta^{11}\text{B}$ to pH_{SW} , with a regression slope of 2.15 compared to 1.46 in *P. astreoides* and *U. tenuifolia* at the 28 °C temperature condition. However, *S. siderea* showed the greatest sensitivity with a slope of the linear regression between $\delta^{11}\text{B}$ and pH_{SW} of 2.52 but was best fit by a nonlinear regression. At 31 °C, it is notable that the relationship between $\delta^{11}\text{B}$ and pH_{SW} within *P. strigosa* was no longer statistically significant, indicating a potential influence of temperature on $\delta^{11}\text{B}$ in this species, although this was not significant in the ANOVA tests described below (Figure 2, Tables S9 and S11).

Table 1. Average Geochemical Data per Experimental Condition.

Species	T (°C)	CO ₂ (µatm)	δ ¹¹ B (‰) ¹	Error (SD)	N *	B/Ca (µmol/mol)	Error (SD)	N	δ ¹³ C (‰) ²	Error (SD)	N
<i>P. astreoides</i>	28	311	23.2	0.9	6	396	54	6	−2.3	0.5	4
	28	405	23.6	0.9	6	437	31	6	−2.6	0.9	4
	28	702	22.7	1.4	5	432	53	4	−5.2	1.5	4
	28	3309	22.1	0.8	6	410	46	6	12.5	3.1	3
	31	288	24.1	0.1	1	389	17	1	−1.4	0.0	1
	31	442	23.4	1.3	5	424	32	5	−2.6	0.7	4
	31	674	23.1	0.4	5	443	82	5	−3.5	1.3	4
	31	3285	22.6	0.5	2	568	51	2	−5.0	1.2	2
<i>P. strigosa</i>	28	312	24.2	0.6	6	496	43	6	−2.2	0.6	5
	28	406	24.5	1.5	5	495	70	4	−1.1	1.5	3
	28	702	23.3	0.7	6	481	35	6	−4.0	0.6	4
	28	3320	22.2	1.3	6	455	41	6	10.9	1.6	4
	31	288	23.9	0.9	4	527	44	4	−1.8	0.6	4
	31	443	23.9	0.8	5	495	50	5	−1.3	0.7	4
	31	674	23.7	0.5	4	528	33	4	−3.4	0.4	4
	31	3284	23.0	1.5	4	530	54	2	−6.4	2.9	4
<i>S. siderea</i>	28	312	24.5	0.7	6	450	26	6	−3.3	0.2	4
	28	405	23.9	0.5	6	436	18	6	−3.9	0.6	4
	28	703	22.7	0.9	6	424	21	6	−6.2	1.1	4
	28	3317	21.8	1.2	6	415	27	6	12.5	1.7	3
	31	288	24.2	0.4	5	467	11	5	−2.6	0.2	3
	31	449	23.4	0.7	6	425	22	6	−2.6	1.4	4
	31	673	22.1	0.7	5	432	10	4	−5.5	1.4	3
	31	3285	21.3	1.4	6	428	21	6	14.3	2.0	3
<i>U. tenuifolia</i>	28	312	24.59	0.68	4	490	51	4	−2.2	0.4	4
	28	404	24.25	0.56	4	518	32	4	−2.6	0.3	4
	28	698	23.54	1.25	4	464	76	4	−3.8	1.0	4
	28	3303	22.53	1.94	4	461	62	4	−7.2	2.8	4

* number of specimens analyzed; ¹ NIST; ² V-PDB.

To further constrain trends in the data, two-way ANOVA tests were used to explore the individual and combined effects of $p\text{CO}_2$ and temperature on geochemical parameters. For *P. astreoides*, $p\text{CO}_2$ alone had a significant individual effect on $\delta^{11}\text{B}$ and $\delta^{13}\text{C}$, while temperature had no effect on geochemical parameters. However, the combined effect of temperature and $p\text{CO}_2$ was found to significantly impact B/Ca. For *P. strigosa*, $p\text{CO}_2$ had a significant effect on $\delta^{11}\text{B}$ and $\delta^{13}\text{C}$, and temperature only influenced B/Ca. In *S. siderea*, $p\text{CO}_2$ had a significant effect on $\delta^{11}\text{B}$, $\delta^{13}\text{C}$, and B/Ca, whereas temperature had an effect on $\delta^{13}\text{C}$ alone. Lastly, in *U. tenuifolia*, only $p\text{CO}_2$ had a significant effect on $\delta^{13}\text{C}$, and no temperature effects were observed. Results of these analyses are presented in Tables 2 and S10.

Coral specimens were collected from both the inshore and offshore reef environments (Supplementary Table S3). Although previous work showed that reef environment had an effect on the physiological response of the corals [39], we found no significant effect of reef environment on the geochemical data or on the carbonate system parameters calculated for the coral calcifying fluid (Table S10). A lack of effect of local reef environment in skeleton boron and carbon geochemistry is a positive feature in terms of using the species as palaeoceanographic archives.

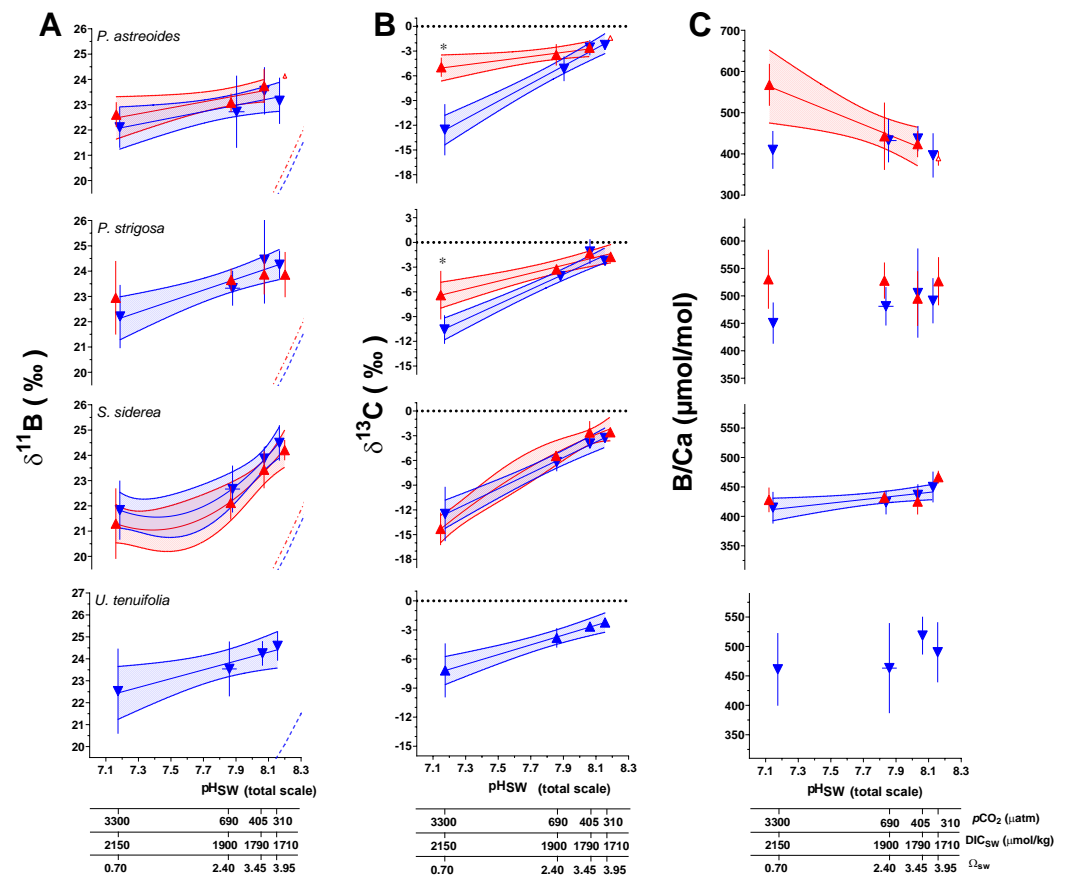


Figure 2. Measured $\delta^{11}\text{B}$ (A), $\delta^{13}\text{C}$ (B), and B/Ca (C) composition of coral aragonite following the 93-day culturing experiment. Large triangular symbols represent the mean value ($\pm 1\text{SD}$) for each treatment condition. Blue symbols represent the control temperature (28 °C) treatment condition and red represents the high temperature (31 °C) treatment condition. Linear versus centered quadratic fit was determined using the Akaike’s Information Criteria test (Table S8), with shaded areas representing the 95% confidence interval. Dashed blue and red curves represent the expected $\delta^{11}\text{B}$ composition of borate ion ($\text{B}(\text{OH})_4^-$) in solution at 28 °C and 31 °C, respectively. * indicates a significant difference between 28 °C and 31 °C data for a given $p\text{CO}_2$ treatment as demonstrated by a p -value < 0.05 in a Welch’s T test.

It is important to note that the principal driver of trends in $\delta^{13}\text{C}$ data across variable $p\text{CO}_2$ and pH_{SW} treatments is the isotopic composition of the CO_2 gas used to manipulate the $p\text{CO}_2$ of the treatment seawater. This gas is combustion sourced and therefore has a relatively negative $\delta^{13}\text{C}$ composition that influences the $\delta^{13}\text{C}$ of DIC more in cultures with higher $p\text{CO}_2$. Despite these trends being influenced by the $\delta^{13}\text{C}$ of the source gas, there is potential to meaningfully interpret the difference between the $\delta^{13}\text{C}$ values between the two temperature treatments for a given $p\text{CO}_2$. For example, Welch’s T-Tests indicate a statistically significant difference in $\delta^{13}\text{C}$ data between the 28 °C and 31 °C treatments at the highest $p\text{CO}_2$ treatment for *P. astreoides* and *P. strigosa*, but not at the lowest $p\text{CO}_2$ condition (Figure 3). Additionally, ANCOVA tests reveal the linear regressions through $\delta^{13}\text{C}$ data as a function of $p\text{CO}_2$ for both *P. astreoides* and *P. strigosa* have significantly different slopes at 28 °C versus 31 °C ($p < 0.0001$ and $p = 0.0021$, respectively), while *S. siderea* did not exhibit a significant change in slope across temperature conditions ($p = 0.102$). These trends in $\delta^{13}\text{C}$ are likely to reflect changes in the sources of DIC for calcification linked to the coral host and symbiont physiological responses to temperature and $p\text{CO}_2$, as further explored in the following sections.

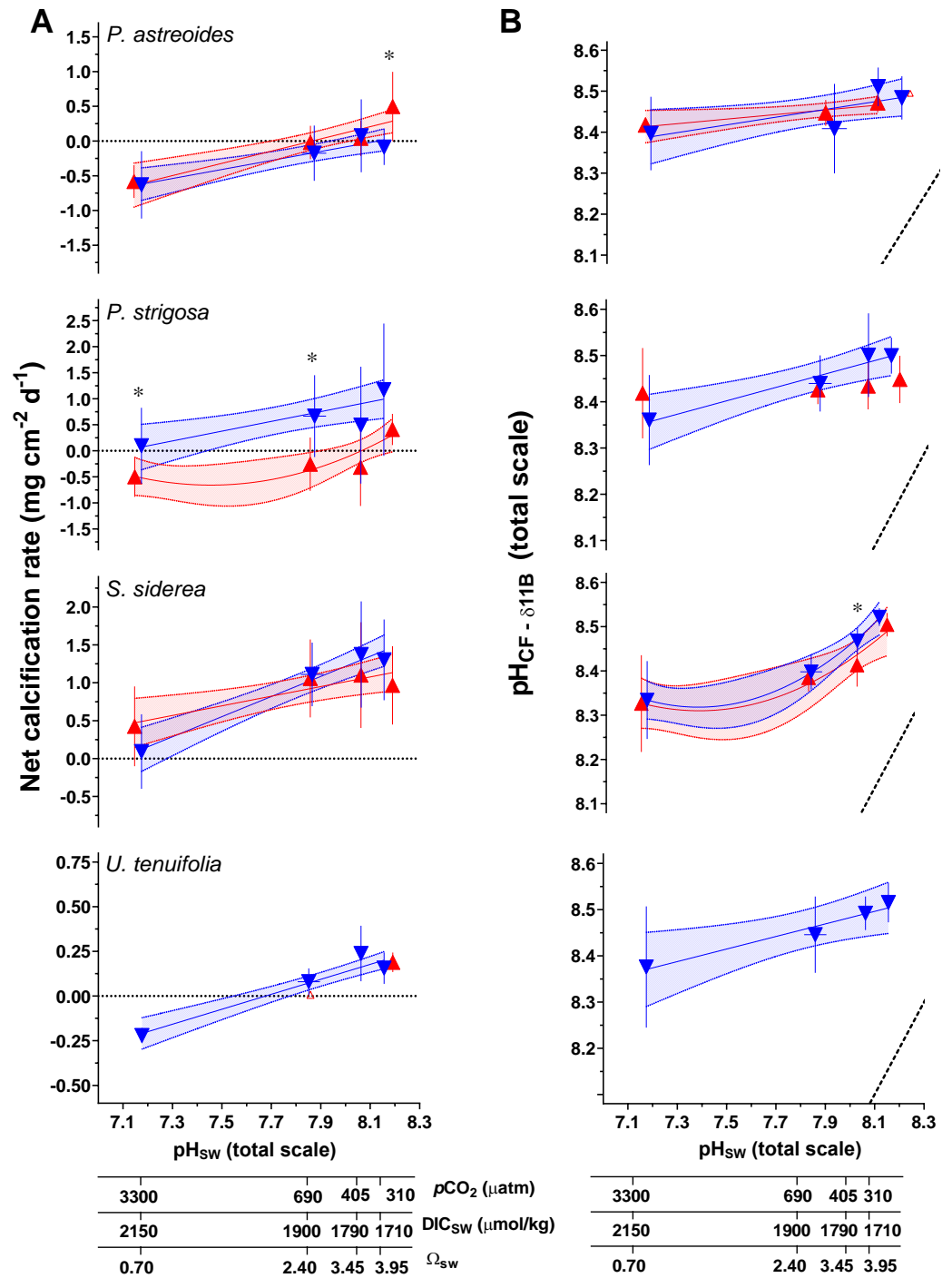


Figure 3. (A) Measured net calcification rate ($\text{mg cm}^{-2} \text{d}^{-1}$), replotted from Bove et al. [38]. (B) $\delta^{11}\text{B}$ -derived pH_{CF} . Triangle symbols represent the mean value (± 1 SD) for each treatment condition, blue and red symbols represent the 28 °C and 31 °C treatments, respectively. Linear versus centered quadratic fit was determined using the Akaike’s Information Criteria test (Table S8), with shading representing the 95% confidence interval. * indicates a significant difference between 28 °C and 31 °C data for a given $p\text{CO}_2$ treatment, as demonstrated by a p -value < 0.05 in a Welch’s T-test.

Table 2. 2-way ANOVA output testing the influence of temperature and $p\text{CO}_2$ on measured geochemical parameters.

Geochemical Parameter	Species	Experimental Variable	ANOVA p -Value		
$\delta^{11}\text{B}$	<i>P. astreoides</i>	Temperature	0.1171		
		CO ₂	0.0152		
		Temperature + CO ₂	0.6094		
	<i>P. strigosa</i>	Temperature	0.5521		
		CO ₂	0.00532		
		Temperature + CO ₂	0.59757		
	<i>S. siderea</i>	Temperature	0.36		
		CO ₂	7.58×10^{-10}		
		Temperature + CO ₂	0.441		
	$\delta^{13}\text{C}$	<i>U. tenuifolia</i>	CO ₂	0.322	
			<i>P. astreoides</i>	Temperature	0.152
				CO ₂	4.12×10^{-5}
Temperature + CO ₂		0.193			
<i>P. strigosa</i>		Temperature	0.5521		
		CO ₂	0.00532		
		Temperature + CO ₂	0.59757		
<i>S. siderea</i>		Temperature	0.36		
		CO ₂	7.58×10^{-10}		
		Temperature + CO ₂	0.441		
B/Ca		<i>U. tenuifolia</i>	CO ₂	0.322	
			<i>P. astreoides</i>	Temperature	0.22201
	CO ₂			0.78951	
	Temperature + CO ₂	0.00939			
	<i>P. strigosa</i>	Temperature	0.00911		
		CO ₂	0.74462		
		Temperature + CO ₂	0.16759		
	<i>S. siderea</i>	Temperature	0.17474		
		CO ₂	0.00103		
		Temperature + CO ₂	0.84438		
	<i>U. tenuifolia</i>	CO ₂	0.484		

3.2. Net Calcification, pH_{CF} , $[\text{CO}_3^{2-}]_{\text{CF}}$, and DIC_{CF}

Net calcification rates for the Caribbean corals were reported in Bove et al. [38], which found that all four coral species showed non-linear reductions in net calcification with increasing $p\text{CO}_2$. Corals showed interspecific differences, with *S. siderea* maintaining positive net calcification under all experimental conditions, *P. strigosa* exhibited a shift to negative net calcification at 31 °C only, and *P. astreoides* exhibited an increase in calcification with elevated temperature at the lower $p\text{CO}_2$ condition, but a shift toward negative calcification (i.e., net dissolution) under the higher $p\text{CO}_2$ treatments (Figure 3).

The pH of the coral calcifying fluid (pH_{CF}) was calculated from $\delta^{11}\text{B}$ data using canonical methods from the literature, as described in the methods section. Although the $\delta^{11}\text{B}$ approach to calculating pH_{CF} in corals has been independently verified based on comparison with pH sensitive dye and pH microelectrode approaches [7,30,47,61,73], significant differences in sensitivities in those approaches appear to exist, and different hypotheses have been advanced to explain these differences [7,47]. At the control temperature and $p\text{CO}_2$ experimental condition (28 °C, 405 $\mu\text{atm } p\text{CO}_2$), mean $\delta^{11}\text{B}$ -derived pH_{CF} (total scale, ± 1 SD) for each species was as follows: *P. astreoides* (8.45 ± 0.06), *P. strigosa* (8.50 ± 0.11), *S. siderea* (8.47 ± 0.03), *U. tenuifolia* (8.49 ± 0.04) (Table 3).

The $[\text{CO}_3^{2-}]_{\text{CF}}$ and DIC_{CF} were calculated from $\delta^{11}\text{B}$ and B/Ca data using the K_{D} of McCulloch et al. [74] and the approach of DeCarlo et al. [51] (Table 3), as described in the methods section. The B/Ca proxy is still prone to uncertainties [70,75] and would benefit from additional validation. One critique is that the proxy is based on limited inorganic precipitation datasets [76,77] which have been difficult to reconcile due to different experimental conditions and from varying $[\text{Ca}^{2+}]$ in the experiment leading in turn

to varying saturation states of aragonite (Ω) within the precipitation experiments [70]. This leads to potential difficulties when translating to highly biologically controlled fluids (such as the calcifying fluid in corals). Additionally, it is possible that coral biomineralization involves transformation of amorphous precursor phases, as evidenced by the detection of amorphous calcium carbonate (ACC) in corals [78], although it is unclear whether this is the universal pathway by which corals calcify. Amorphous or metastable phases of calcium carbonate may have different K_D , which could contribute to differences in biomineral chemistry [79,80], although given that ACC transformation seems to occur via dissolution and reprecipitation into crystalline phases [81], precursor phase K_D may not be relevant for the final mineral. Despite these uncertainties, results of Guillermic et al. [7] showed that the K_D formulations used by DeCarlo et al. [51] (Termed D18); McCulloch et al. [74] (M17); Holcomb et al. [77] (H16) resulted in similar reconstructed $[\text{CO}_3^{2-}]_{\text{CF}}$ among biological replicates and that the outcome was within error of independent measurements from $[\text{CO}_3^{2-}]$ microelectrodes as reported by Sevilgen et al. [35] (S19) for the same coral species (*S. pistillata*) (M17: 909 ± 313 (SD, $n = 8$), H16: 757 ± 342 (SD, $n = 8$), D18: 848 ± 392 (SD, $n = 7$), S19: 679 ± 183 (SD); at 311 ppm $p\text{CO}_2$, 28 °C) [7].

Regression analysis of net calcification, calculated pH_{CF} , $[\text{CO}_3^{2-}]_{\text{CF}}$, and DIC_{CF} as a function of pH_{SW} were explored using an AIC approach (Figures 3 and 4; Table S9). pH_{CF} as a function of pH_{SW} follows a similar pattern to the originating $\delta^{11}\text{B}$ data (Figure 3; Table S9). Patterns in $[\text{CO}_3^{2-}]_{\text{CF}}$ as a function of pH_{SW} differ from patterns in pH_{CF} as a function of pH_{SW} , with only *P. strigosa* and *S. siderea* showing statistically significant regressions under the 28 °C treatment (Figure 4; Table S9).

In addition, regression analyses of net calcification as a function of pH_{CF} , $[\text{CO}_3^{2-}]_{\text{CF}}$, and $[\text{DIC}]_{\text{CF}}$ were explored using the AIC approach. Here, linear regressions were typically favored but rarely reached statistical significance (Table S9). This result is not surprising given the previous findings of Liu et al. [69] that pH_{CF} is not necessarily tightly coupled to net calcification responses to seawater acidification in a wide range of marine calcifiers, including the temperate coral *Oculina arbuscula*. Net calcification represents a balance of dissolution and calcification and will be influenced by both physicochemical and other controls over calcification, all of which may confound a clear relationship with pH_{CF} .

Two-way ANOVA tests were again used to explore the individual and combined effects of $p\text{CO}_2$ and temperature on calculated calcifying fluid parameters of pH_{CF} , $[\text{CO}_3^{2-}]_{\text{CF}}$, and DIC_{CF} . In *P. astreoides*, $p\text{CO}_2$ had a significant effect on pH_{CF} and $[\text{CO}_3^{2-}]_{\text{CF}}$. Temperature and the combined effect of temperature and $p\text{CO}_2$ had significant effects on DIC_{CF} . Similarly, in *P. strigosa*, $p\text{CO}_2$ had a significant effect on pH_{CF} and $[\text{CO}_3^{2-}]_{\text{CF}}$, but temperature only had an individual effect on DIC_{CF} . In *S. siderea*, the calculated pH_{CF} data did not meet assumptions of normality after transformation and, consequently, ANOVA results are not presented. There was a significant effect of $p\text{CO}_2$ on $[\text{CO}_3^{2-}]_{\text{CF}}$ of *S. siderea* and significant individual effects of both $p\text{CO}_2$ and temperature on DIC_{CF} . Lastly, *U. tenuifolia* displayed no significant effects of either $p\text{CO}_2$ or temperature on the calculated calcifying fluid parameters. Results of these analyses are presented in Table 4.

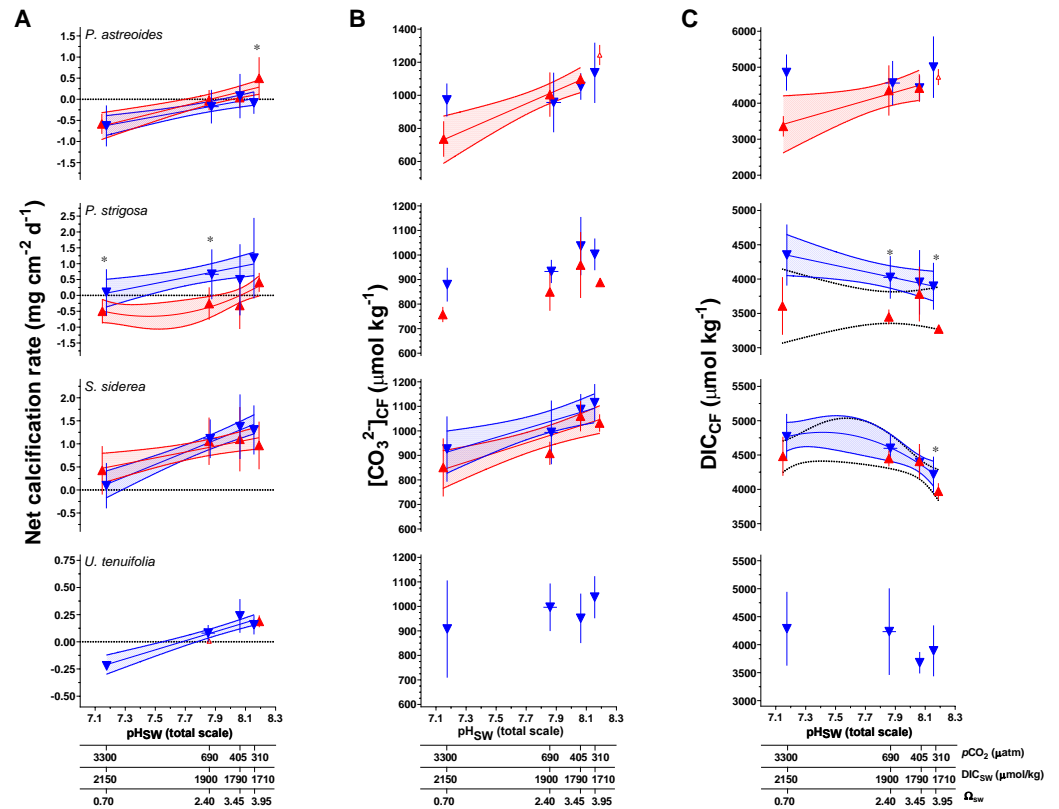


Figure 4. (A) Measured net calcification rate ($\text{mg cm}^{-2} \text{d}^{-1}$) replotted from Bove et al. [38] (B) B/Ca-derived carbonate ion concentration of the coral calcifying fluid ($[\text{CO}_3^{2-}]_{\text{CF}}$, $\mu\text{mol/mol}$), and (C) combined $\delta^{11}\text{B}$ and B/Ca-derived dissolved inorganic carbon concentration of the coral calcifying fluid (DIC_{CF} , $\mu\text{mol/mol}$). Triangle symbols (± 1 SD) represent the mean value for each treatment condition, blue and red symbols represent the 28 °C and 31 °C treatment conditions, respectively. Linear versus centered quadratic fit was determined using the Akaike Information Criteria test (Table S8), with shading representing the 95% confidence interval. * indicates a significant difference between 28 °C and 31 °C data for a given $p\text{CO}_2$ treatment, as demonstrated by a p -value < 0.05 in a Welch’s-T test.

Table 3. Net calcification data and calculated calcifying fluid pH and carbonate system parameters.

Species	T (°C)	CO ₂ (μatm)	Net Calcification (mg cm ⁻² d ⁻¹)	Error (SD)	N ¹	pH _{CF}	Error (SD)	DIC _{CF} (mmol/mol)	Error (SD)	[CO ₃ ²⁻] _{CF} (mmol/mol)	Error (SD)	Ω _{CF} ²	Error (SD)	N	
<i>P. astreoides</i>	28	311	-0.08	0.26	11	8.42	0.06	4983	863	1131	181	20.9	3.4	6	
	28	405	0.07	0.52	12	8.45	0.06	4421	352	1053	81	19.5	1.5	6	
	28	702	-0.17	0.4	10	8.39	0.10	4561	618	957	180	17.8	3.3	4	
	28	3309	-0.65	0.5	12	8.35	0.05	4841	512	969	102	17.9	1.9	6	
	31	288	0.5	0.5	6	8.45	0	4777	0	1242	0	23	0	1	
	31	442	0.04	0.29	8	8.40	0.09	4434	394	1055	107	19.5	2	5	
	31	674	-0.02	0.24	9	8.38	0.02	4365	703	1004	133	18.6	2.5	5	
	31	3285	-0.54	0.27	3	8.35	0.03	3356	286	736	106	13.6	2	2	
	<i>P. strigosa</i>	28	312	0.92	1.28	13	8.49	0.04	3862	362	989	59	18.3	1.1	6
		28	406	1	1.12	6	8.50	0.10	3881	590	1013	85	18.7	1.6	4
28		702	0.66	0.79	14	8.43	0.04	4025	311	933	47	17.3	0.9	6	
28		3320	0.03	0.71	16	8.36	0.08	4339	452	876	68	16.2	1.3	6	
31		288	0.41	0.3	9	8.43	0.06	3269	9	889	12	16.4	0.2	2	
31		443	-0.32	0.74	6	8.43	0.05	3782	399	959	134	17.8	2.5	5	
31		674	-0.23	0.55	7	8.42	0.03	3450	109	850	78	15.7	1.4	3	
31		3284	-0.5	0.39	8	8.37	0.10	3609	423	759	35	14	0.6	2	

Table 3. Cont.

Species	T (°C)	CO ₂ (µatm)	Net Calcification (mg cm ⁻² d ⁻¹)	Error (SD)	N ¹	pH _{CF}	Error (SD)	DIC _{CF} (mmol/mol)	Error (SD)	[CO ₃ ²⁻] _{CF} (mmol/mol)	Error (SD)	Ω _{CF} ²	Error (SD)	N
<i>S. siderea</i>	28	312	1.30	0.57	10	8.51	0.05	4216	261	1115	76	20.6	1.4	6
	28	405	1.37	0.70	12	8.47	0.03	4391	192	1087	63	20.1	1.2	6
	28	703	1.08	0.45	11	8.39	0.06	4596	194	993	129	18.4	2.4	6
	28	3317	0.13	0.52	11	8.33	0.08	4765	333	926	133	17.1	2.5	6
	31	288	1.00	0.54	8	8.46	0.03	3969	117	1033	34	19.1	0.6	4
	31	449	1.16	0.70	11	8.41	0.05	4407	252	1060	62	19.6	1.1	6
	31	673	1.06	0.51	11	8.32	0.05	4449	120	909	47	16.8	0.9	3
	31	3285	0.43	0.53	12	8.26	0.10	4480	284	851	119	15.7	2.2	5
<i>U. tenuifolia</i>	28	312	0.16	0.10	11	8.52	0.04	3886	449	1037	85	19.2	1.6	4
	28	404	0.24	0.17	7	8.49	0.04	3676	188	950	102	17.6	1.9	4
	28	698	0.05	0.08	4	8.44	0.08	4230	767	996	99	18.5	1.8	4
	28	3303	-0.23	0.05	5	8.38	0.13	4286	657	908	198	16.8	3.7	4

¹ Refers to number of specimens analyzed; ² Ω_{CF} values calculated using the assumption of [Ca]_{CF} = [Ca]_{SW}.

Table 4. 2-way ANOVA output testing the influence of temperature and pCO₂ on calculated calcifying fluid carbonate system parameters and coral and symbiont physiological parameters.

Parameter/Species/Experimental Variable	p Value	p Value	
Symbiont cell density		pH_{CF}	
<i>P. astreoides</i>		<i>P. astreoides</i>	
Temperature	0.417	Temperature	0.676
CO ₂	0.11	CO ₂	6.54 × 10⁻⁵
Temperature + CO ₂	0.466	Temperature + CO ₂	0.286
<i>P. strigosa</i>		<i>P. strigosa</i>	
Temperature	2.59 × 10⁻¹¹	Temperature	0.42275
CO ₂	0.648	CO ₂	0.00536
Temperature: CO ₂	0.15	Temperature + CO ₂	0.62005
<i>S. siderea</i>		<i>S. siderea</i>	
Temperature	9.09 × 10⁻⁵	Temperature	Not Normal *
CO ₂	0.000251	CO ₂	Not Normal *
Temperature + CO ₂	0.858348	Temperature + CO ₂	Not Normal *
<i>U. tenuifolia</i>		<i>U. tenuifolia</i>	
CO ₂	0.727	CO ₂	0.317
Chl a		[CO₃²⁻]	
<i>P. astreoides</i>		<i>P. astreoides</i>	
Temperature	9.89 × 10⁻⁷	Temperature	0.41309
CO ₂	6.10 × 10⁻¹¹	CO ₂	0.00333
Temperature + CO ₂	2.80 × 10⁻⁹	Temperature + CO ₂	0.22932
<i>P. strigosa</i>		<i>P. strigosa</i>	
Temperature	6.15 × 10⁻⁸	Temperature	0.0988
CO ₂	0.000217	CO ₂	0.0224
Temperature: CO ₂	0.070441	Temperature: CO ₂	0.855
<i>S. siderea</i>		<i>S. siderea</i>	
Temperature	0.00394	Temperature	0.679
CO ₂	1.37 × 10⁻⁷	CO ₂	5.98 × 10⁻⁵
Temperature + CO ₂	0.25756	Temperature + CO ₂	0.996
<i>U. tenuifolia</i>		<i>U. tenuifolia</i>	
CO ₂	0.033	CO ₂	0.181
Total host energy		[DIC]_{CF}	
<i>P. astreoides</i>		<i>P. astreoides</i>	
Temperature	0.02755	Temperature	0.00163
CO ₂	0.00659	CO ₂	0.69095
Temperature: CO ₂	0.06197	Temperature + CO ₂	0.04313
<i>P. strigosa</i>		<i>P. strigosa</i>	
Temperature	8.35 × 10⁻⁵	Temperature	0.00395
CO ₂	0.103	CO ₂	0.26074
Temperature + CO ₂	0.857	Temperature + CO ₂	0.3616

Table 4. Cont.

Parameter/Species/Experimental Variable			p Value		
<i>S. siderea</i>	Temperature	0.000522	<i>S. siderea</i>	Temperature	0.00119
	CO ₂	0.118746		CO ₂	2.62×10^{-5}
	Temperature + CO ₂	0.710086		Temperature + CO ₂	0.3765
<i>U. tenuifolia</i>	CO ₂	0.168	<i>U. tenuifolia</i>	CO ₂	0.463
	Calcification rate				
<i>P. astreoides</i>	Temperature	0.0178	<i>P. strigosa</i>	Temperature	0.000142
	CO ₂	5.11×10^{-6}		CO ₂	0.000364
	Temperature + CO ₂	0.1779		Temperature + CO ₂	0.678234
<i>S. siderea</i>	Temperature	0.52	<i>S. siderea</i>	Temperature	0.52
	CO ₂	3.27×10^{-8}		CO ₂	3.27×10^{-8}
	Temperature + CO ₂	0.209		Temperature + CO ₂	0.209

* Data did not reach normality even after transformation steps, so ANOVA test was not performed.

We combined our data with a compilation of coral data from the literature using different approaches (geochemistry, microelectrode, pH-sensitive dye; Table S11). It is clear from almost all published studies that pH_{CF}, [CO₃²⁻]_{CF}, and DIC_{CF} are differentiated from seawater values and that this is an active compensatory process as pH_{CF}, and [CO₃²⁻]_{CF} values are increasingly elevated relative to seawater values under acidified conditions (Figures 5 and 6).

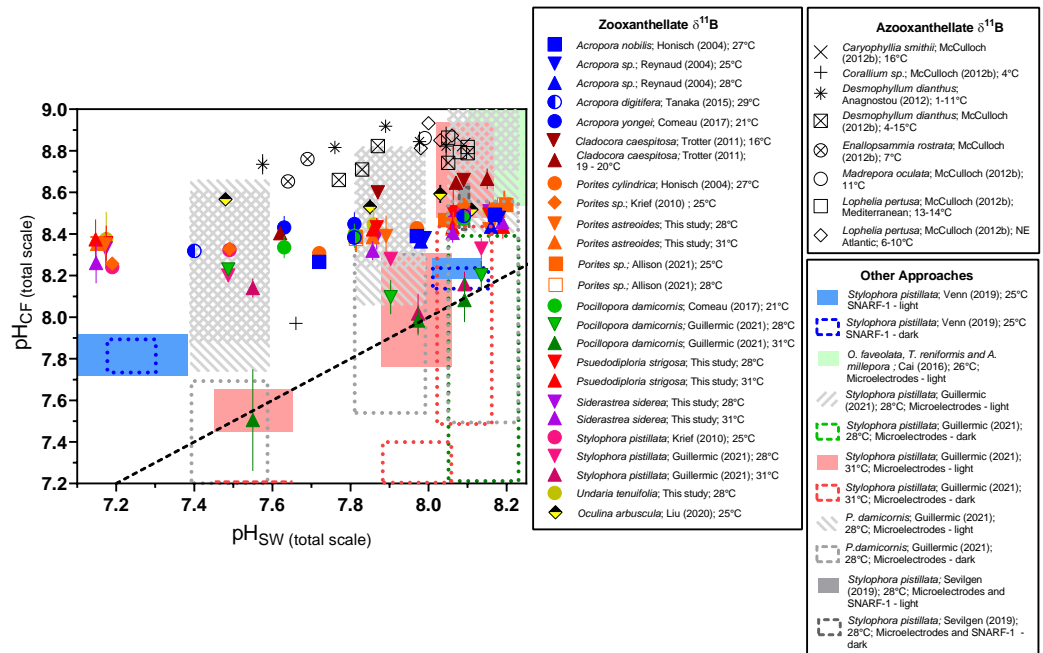


Figure 5. Compilation of δ¹¹B-derived calcification fluid pH_{CF} data from shallow-water zooxanthellate coral culturing experiments. We include data from cold-water azooxanthellate corals as a point of reference, as well as ranges of pH_{CF} data as determined by SNARF pH-sensitive dyes and pH microelectrode analyses. ‘RR’ label denotes corals treated with the Ca-ATPase inhibitor ruthenium red [32]. Previously published data used in the figure are available in Table S12 alongside citations for data sources.

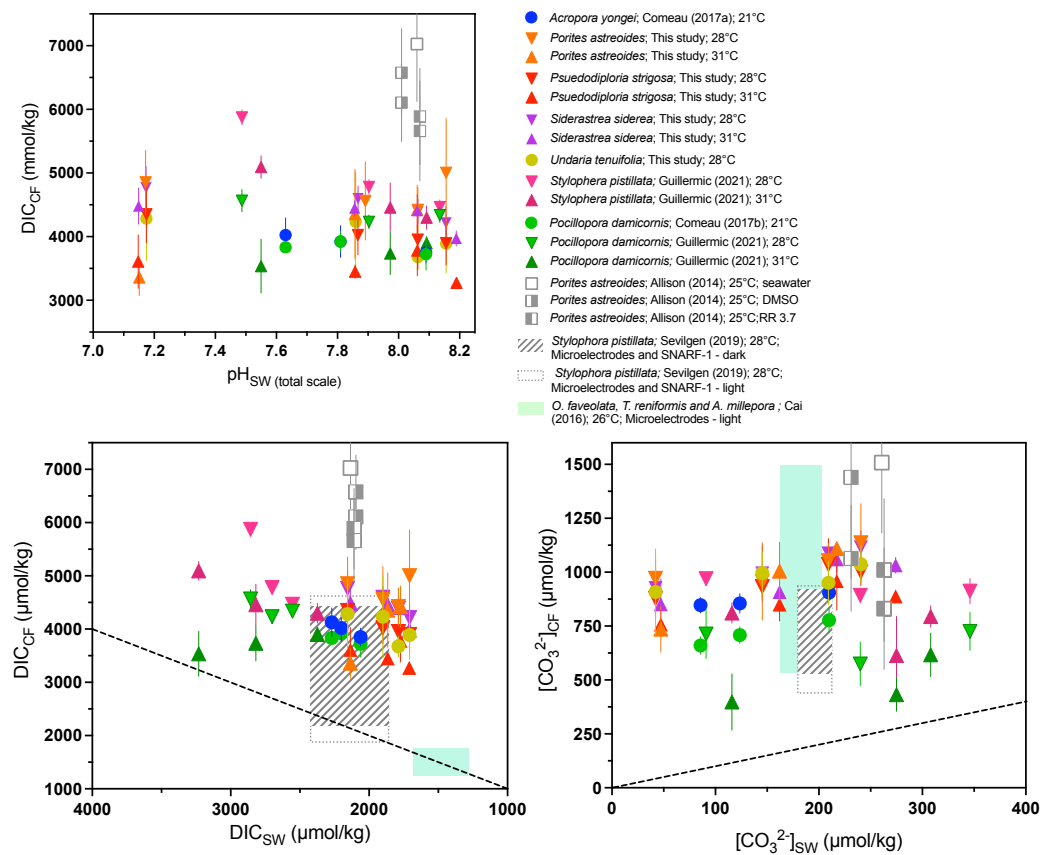


Figure 6. Compilation of combined $\delta^{11}\text{B}$ and B/Ca-derived DIC_{CF} and $[\text{CO}_3^{2-}]_{\text{CF}}$ measurements from available published data, as well as published microelectrode data. We include cultured shallow-water zooxanthellate corals, cold-water azooxanthellate corals, as well as a range of DIC_{CF} values as determined by SNARF-1 pH-sensitive dyes and pH microelectrode analyses. (A) DIC_{CF} as a function of pH_{SW} (total scale), (B) DIC_{CF} as a function of DIC_{SW} , and (C) $[\text{CO}_3^{2-}]_{\text{CF}}$ as a function of $[\text{CO}_3^{2-}]_{\text{SW}}$. ‘RR’ label denotes corals treated with the Ca-ATPase inhibitor ruthenium red [32]. Previously published data used in the figure are available in Table S12 alongside citations for data sources.

3.3. Biological Compensation for External pH Changes, and the Importance of Coral and Symbiont Physiology

Changes in pH_{CF} across experimental conditions are relatively small, with values changing, for example, from 8.52 to 8.26 in the most sensitive coral species *S. siderea*. However, it is important to note that this represents a substantial compensation or buffering by the coral with respect to the much larger changes in pH_{SW} , which range from 8.3 to 7.3 in the experiment.

To illustrate the chemical effects of this compensation, we provide calculations of the proton differential ($[\text{H}^+]_{\text{SW}} - [\text{H}^+]_{\text{CF}}$), maintained by the coral with respect to seawater under all experimental conditions (Figure 7, Table S9), for which larger values represent a greater difference in proton concentration in the calcification fluid relative to seawater. For example, for *P. astreoides* at 28 °C, the comparison between the 311 $\mu\text{atm } p\text{CO}_2$ and the $\sim 33,309 \mu\text{atm } p\text{CO}_2$ treatments show a proton differential of $0.5 \times 10^{-8} \text{ mol/L}$ at 400 $\mu\text{atm } p\text{CO}_2$ and $6.3 \times 10^{-8} \text{ mol/L}$ at 3000 μatm , which represents a differential 12.4 times higher at the elevated $p\text{CO}_2$ condition. At 31 °C for *P. astreoides*, the differential is 13.4 times higher between the $\sim 400 \mu\text{atm}$ and $\sim 3000 \mu\text{atm } p\text{CO}_2$ conditions. The same comparison shows a proton differential 11.4 and 13.4 times higher for *P. strigosa* at 28 °C and 31 °C, 11.9 and 13.9 times higher for *S. siderea* at 28 °C and 31 °C and 11.5 times higher for *U. tenuifolia* at 28 °C.

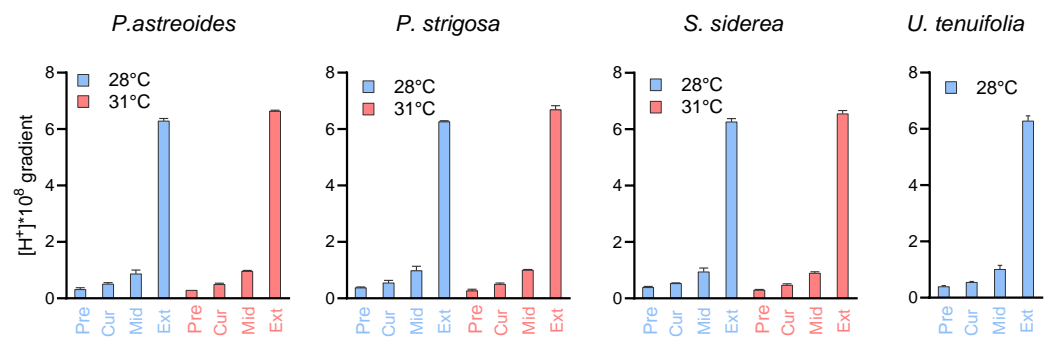


Figure 7. Proton differentials maintained by the coral species between seawater and their calcifying fluid ($[H^+]_{SW} - [H^+]_{CF}$). Values are given for preindustrial, present day, mid-century, and extreme (~3300 ppm) pCO_2 conditions, with precise pCO_2 values given in Table S1. Calculated values are provided in Table S9.

Using the compilation of pH_{CF} data from the literature and from the present study, we compare the slopes of the relationships between pH_{CF} and pH_{SW} (Figure 8), with a slope of 1 indicating that changes in pH_{CF} perfectly track changes in pH_{SW} , and a slope of 0 indicating that the coral is perfectly compensating for external changes in pH_{SW} and that pH_{CF} is invariant across the experimental conditions. This compilation demonstrates that although there are cases where corals perfectly compensate for external pH_{SW} changes, in most cases corals exhibit a modest decrease in pH_{CF} with decreasing pH_{SW} (Figure 8). Furthermore, $\delta^{11}B$ -based estimates of pH_{CF} were generally lower than that found by the microelectrode approach (Figure 8). We hypothesized in previous work that this could reflect different time intervals being recorded by these approaches [7], but it cannot be ruled out that there are systematic differences in the techniques, such as recording different microenvironments.

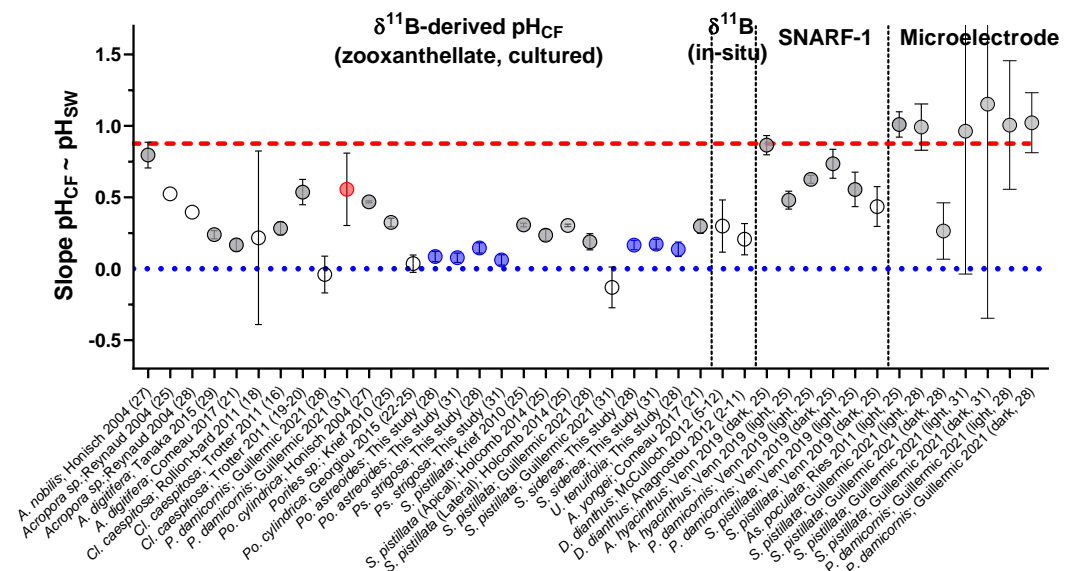


Figure 8. The sensitivity of pH_{CF} to pH_{SW} within the coral species studied here and reported in the literature. Y-Axis is the slope of the relationship between pH_{CF} and pH_{SW} , with a value of 1 showing that change in pH_{CF} directly tracks the magnitude of the change in pH_{SW} , and a value of 0 indicating perfect control over coral pH_{CF} amidst variable pH_{SW} . On X axis, numbers in parenthesis are the temperature of the experiment. Previously published data used in the figure are available in Table S12 alongside citations for data sources.

It should ultimately be Ω_{CF} that is the most influential factor in coral calcification. If pH_{CF} modestly decreases, but Ω_{CF} remains high enough to support efficient coral calcification, then this may explain how corals continue calcifying despite acidification of their calcifying fluid. Calculating Ω_{CF} requires an additional assumption due to the lack of constraints on $[Ca^{2+}]_{CF}$. We conducted a set of calculations where $[Ca^{2+}]_{CF}$ is assumed to be equivalent to $[Ca^{2+}]_{SW}$ (Table 2 and Table S7). The calculated saturation states were then plotted against coral calcification data (Figure 9). Our compilation of Ω_{CF} exhibits inter-species variation, but none of the four species (*S. siderea*, *P. strigosa*, *P. astreoides* and *U. tenuifolia*) exhibit significantly different values from each other at under control temperature and pCO_2 conditions (ANOVA test, $p = 0.2$), but were significantly higher compared to that calculated for *S. pistillata* [7], *A. yongei* ($p < 0.05$) and *P. damicornis* ($p < 0.05$) [7,67] using the same assumptions. Species-specific threshold values of Ω_{CF} , where calcification is outweighed by dissolution, can be estimated from Figure 9, but care should be taken interpreting those absolute values due to the lack of constraints on $[Ca^{2+}]_{CF}$. There is a possibility that $[Ca^{2+}]_{CF}$ could differ between species, as highlighted by previous work on *A. yongei* and *P. damicornis* [51]. In addition, the highest calculated Ω_{CF} values do not translate to highest calcification rates for the corals, which may reflect prior observations that coral calcification is complex process beyond simple physicochemical manipulation of the calcifying fluid [78,82].

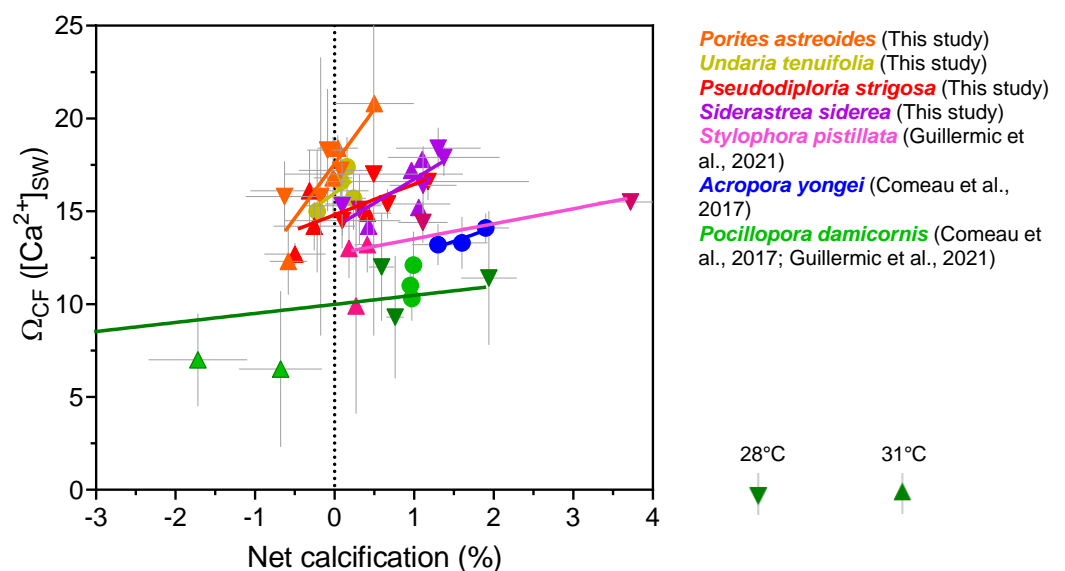


Figure 9. Relationships between boron isotope derived Ω_{CF} and net calcification rates. Ω_{CF} is calculated assuming that $[Ca^{2+}]$ of seawater is equivalent to $[Ca^{2+}]$ of the calcifying fluid. Published data used in this figure is given in Table S12 with citations for data sources.

Statistical analyses of coral and symbiont physiological data from this experiment have been explored elsewhere [39]. Here, we perform additional 2-way ANOVA tests on the same data to produce statistical tests that are handled identically between the geochemical and physiological data. In *P. astreoides*, we found significant individual and combined effects of pCO_2 and temperature on Chl a, and total host energy reserves, but not on symbiont cell density. Significantly, and as noted in previous work of Bove et al. [39], the significant effect of temperature on Chl a in *P. astreoides* is actually to increase levels, whereas for all other significant effects reported from our ANOVA test they are characterizing decreases. However, it is important to note that temperature actually improved symbiont physiological parameters in this species, rather than repressing them as reported previously for this species [39]. In *P. strigosa*, only temperature had an effect on both symbiont cell density and total host energy reserves. Significant individual effects of both temperature and pCO_2 on both symbiont cell density and Chl a were observed for *S. siderea*, whilst only temperature had an effect on total host energy for this species. For *U. tenuifolia*, only pCO_2

had an effect on Chl a. Results of these analyses are presented in Table 4. Specimens of *S. siderea* were collected from both the inshore and offshore environments and previous work showed that reef environment affected physiological response; however, our results show a nonsignificant effect of reef environment on physiological data (Table S10), which likely reflects the difference in statistical approaches, with ANOVA tests employed here on single parameters versus the principal component analyses conducted by Bove et al. [39].

These physiological data are relevant for understanding how host and symbiont responses to environmental change may influence the chemistry of the calcifying fluid. It is notable that in the three coral species examined (excluding *U. tenuifolia*), temperature was found to influence total host energy reserves, or the total of the lipid, carbohydrate, and protein concentrations for a given area of coral host tissue. Temperature was not found to influence pH_{CF} and $[\text{CO}_3^{2-}]_{\text{CF}}$, but in all three corals was found to reduce $[\text{DIC}]_{\text{CF}}$ (Table 4). Whilst this observation does not prove cause and effect, it is consistent with temperature stress causing depletion of host energy reserves, and reduced host input of respiration produced CO_2 into the DIC pool for calcification. As temperature increase was associated with reduced symbiont cell density and Chl a in some of the corals, this is consistent with a scenario where the symbiont was less efficiently supplying energy to the host, leading to the observed decrease in energy reserves.

To further explore the relationship between these host and symbiont physiological changes and the source of carbon in the calcification fluid, we examined $\Delta\delta^{13}\text{C}$ ($\delta^{13}\text{C}_{31^\circ\text{C}} - \delta^{13}\text{C}_{28^\circ\text{C}}$) for each $p\text{CO}_2$ treatment. In Figure 10, $\Delta\delta^{13}\text{C}$ is plotted against $\Delta[\text{DIC}]$ ($[\text{DIC}]_{31^\circ\text{C}} - [\text{DIC}]_{28^\circ\text{C}}$). This analysis shows that, on one hand, there is a significant difference in the source of carbon for calcification between *S. siderea* and *S. pistillata*, for which temperature did not influence $\delta^{13}\text{C}$ at the higher $p\text{CO}_2$ conditions. On the other hand, it shows that at higher $p\text{CO}_2$ conditions, $\Delta\delta^{13}\text{C}$ of *P. astreoides* and *P. strigosa* (Figure 10) shifted to more positive values and that $\Delta[\text{DIC}]$ shifted towards more negative values compared to the other corals, with the overall effect most pronounced in *P. astreoides*. The potential mechanisms driving these trends are discussed below.

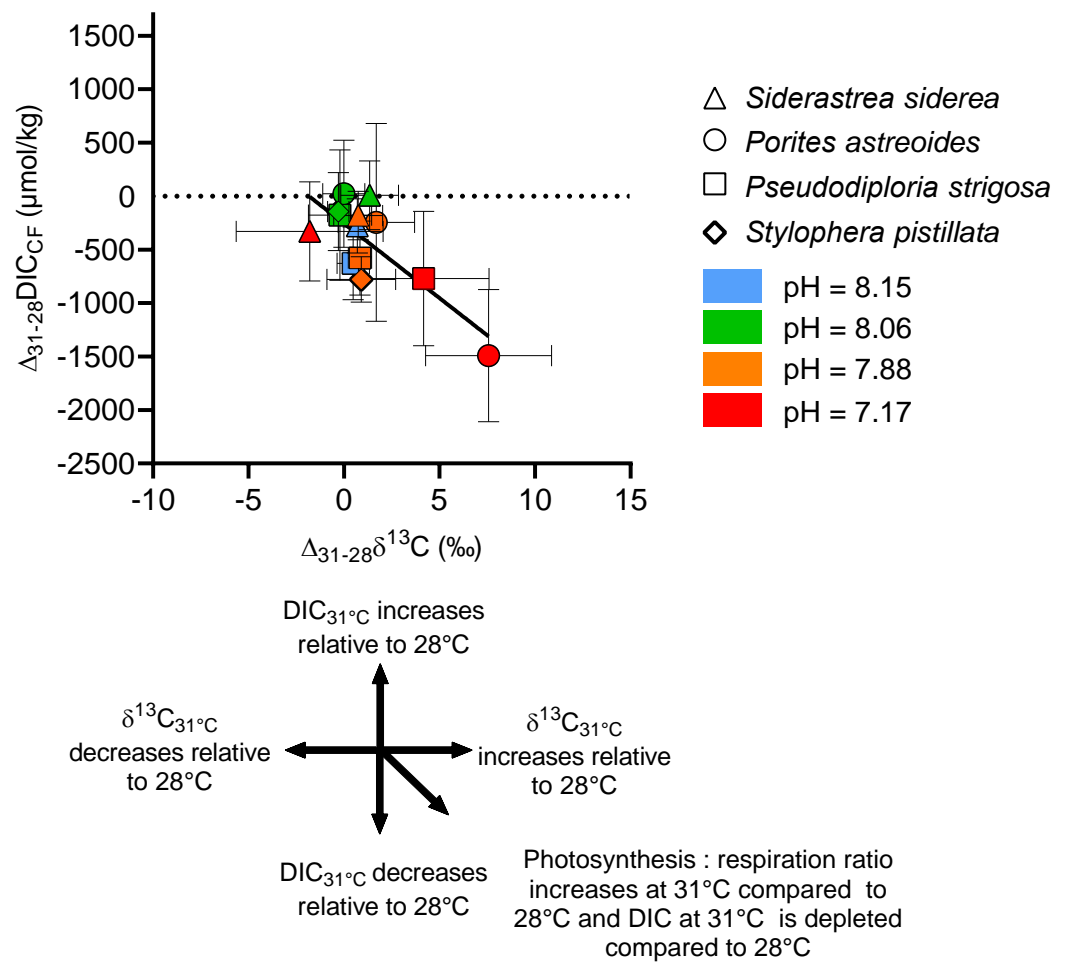


Figure 10. Combined influence of temperature and pCO_2 on the $\delta^{13}C$ and [DIC] of the coral calcifying fluid. Data are expressed as $\Delta\delta^{13}C$ ($\delta^{13}C_{31^\circ C} - \delta^{13}C_{28^\circ C}$) and $\Delta[DIC]$ ($[DIC]_{31^\circ C} - [DIC]_{28^\circ C}$) for each pCO_2 treatment.

4. Discussion

Collectively, the data from this study and the literature suggest that most corals experience a degree of acidification of their internal calcification fluid media in response to external seawater acidification. Nonetheless, considerable biological compensation is observed for the studied species, which maintain a larger proton differential between the calcifying fluid and seawater under elevated pCO_2 . Therefore, the slight decreases in pH_{CF} under elevated pCO_2 may represent either a practical tradeoff by the coral, or a biological limit to controlling calcifying fluid chemistry that still allows the coral to maintain $[CO_3^{2-}]_{CF}$ and Ω_{CF} at a level that supports efficient calcification. The hypothesis that this is an active and energy-consuming adaptation by corals is supported by the finding that the ability of corals to regulate pH and carbonate chemistry of their calcifying fluid can be impaired by thermal stress and symbiont loss [7,25]. In contrast to our studies of *S. pistillata* and *P. damicornis* [7,25], we found that temperature did not result in a statistically significant change in pH_{CF} regulation across all conditions in the Caribbean species investigated here, although it did under a subset of the experimental conditions in *S. siderea*. This may reflect that the highest temperature treatment in the present experiment [38,39], did not elicit as severe an effect on the corals and their symbionts as in the prior experiment [7,25], with the exception of *U. tenuifolia* that had too high a mortality at elevated temperature to be examined. Notably, the Ca-ATPase inhibitor experiments of Allison et al. [32], and the heat stress experiments of Guillermic et al. [7], on *Pocillopora damicornis* are the only experiments

where corals appeared to almost completely lose the ability to elevate pH_{CF} relative to seawater, as shown in Figure 5.

Furthermore, we are able to examine associations between coral and symbiont physiological responses and calcifying fluid regulation. This revealed a significant depletion in total host energy reserves at elevated temperature, as well as a reduction in $[\text{DIC}]_{\text{CF}}$ in all three corals examined. The reduction in calculated $[\text{DIC}]_{\text{CF}}$ with temperature increase was also seen in the *S. pistillata* and *P. damicornis* experiment described in Guillermic et al. [7]. This result is consistent with a reduction in the energy transfer between the symbiont and host leading to the host depleting its energy reserves and/or the host consuming more energy in response to temperature stress. Although we cannot prove cause and effect, changes in the energy balance between host and symbiont could then lead to a reduction in the production of metabolic CO_2 that is contributed to the DIC pool for calcification, which is consistent with the reduction we see in calculated $[\text{DIC}]_{\text{CF}}$ in these corals. The story is also more complex, however, with additional interactions apparent from the $\delta^{13}\text{C}$ data.

Although the $\delta^{13}\text{C}$ data did not indicate major differences in host and symbiont physiological influence on $[\text{DIC}]_{\text{CF}}$ for the different coral species under the control CO_2 conditions, significant differences in $\delta^{13}\text{C}$ emerged under elevated temperature and CO_2 amongst the species, with shifts towards positive $\delta^{13}\text{C}$ associated with amplified reductions in $[\text{DIC}]_{\text{CF}}$ in two of the coral species studied.

It is thought that changes in the flux of carbon to and from photosynthesis and respiration, respectively, may change the $\delta^{13}\text{C}$ of the DIC pool used for calcification. Photosynthesis preferentially consumes ^{12}C , which may then result in ^{13}C enrichment in the DIC pool for calcification if this pool acts as a source of CO_2 for photosynthesis [83]. As the rate of photosynthesis increases and/or the rate of respiration decreases, the DIC pool should have more positive $\delta^{13}\text{C}$ resulting in more positive coral skeletal $\delta^{13}\text{C}$ [83,84]. In the present experiment, we can see that host respiration input is likely decreasing as the host consumes energy reserves at elevated temperature. There is also an overall reduction in $[\text{DIC}]_{\text{CF}}$, which is likely due to a reduction in CO_2 -input from respiration. One way to explain the relationship between the $\Delta\delta^{13}\text{C}$ and $\Delta[\text{DIC}]$ data in Figure 10 is that, in addition to the reduction in respiration-sourced CO_2 to the DIC pool for calcification, photosynthetic drawdown of $^{12}\text{CO}_2$ by the symbiont is significantly enriching the $\delta^{13}\text{C}$ of the DIC pool in *P. astreoides* and *P. strigosa* at highest temperature and pCO_2 conditions, which could further deplete $[\text{DIC}]_{\text{CF}}$ and drive more positive $\Delta\delta^{13}\text{C}$. This effect was not seen in a similar experiment on *S. pistillata* [7] where symbiont loss and bleaching of the coral occurred [25], which suggests that photosynthetic influence over the DIC pool was minimal at the higher temperature and pCO_2 conditions. This interpretation is also congruent with observations from this experiment that the symbiont in *P. astreoides* is not negatively impacted by increased temperature [39] and is evidence for a divergent host and symbiont physiological response to environmental parameters in this coral species. Conversely, the effects of host respiration and symbiont photosynthesis remained relatively balanced in terms of their influence on the source of DIC for calcification in *S. siderea*. It has been previously noted that *P. astreoides*, *S. siderea*, and *P. strigosa* host differing algal symbiont communities which may result in differing carbon allocation between the host and symbiont [39]. For example, *S. siderea* mainly hosts *Cladocopium* and *Breviolum* whereas *P. astreoides* hosts *Breviolum* and *Symbiodinium* [39]. The potential changes in carbon flux between the host and symbiont is interesting to consider in the context of the debate on the extent of mutualism between the coral host and symbiont, and whether the symbiont develops features that are more parasitic in nature under environmental change [39,85,86].

Overall, the results presented here and in previous work on these corals [7,38,39,87] highlight the considerable complexity in host and symbiont responses to ocean warming and acidification, demonstrating that these responses are closely coupled to a coral's physicochemical control of their calcification process. The combined physiological data from this study, preceding studies [38,39,87], as well as the work of other groups (e.g., [88]), converge on the conclusion that *S. siderea* is a relatively resilient species to environmental

change and so may be amongst the least impacted by future warming and acidification, compared to a number of more sensitive Caribbean species studied such as *O. faveolata*, *M. cavernosa*, and *U tenuifolia* [38,88]. Some differences in observations on *P. astreoides* between studies exist in its temperature sensitivity [38,88] which may reflect intraspecific differences in host or symbiont physiology, with the evidence here suggesting thermal sensitivity can be relatively low for the symbiont of at least some Caribbean *P. astreoides* but that reductions in net calcification can still occur in non-bleached corals in acidified seawater.

The type of data presented here provides useful insights into the underlying physiological mechanisms of coral adaptation, and the variation in responses between species in an experiment. Whilst difficult to make regional or global predictions from single studies, a recent meta-analysis of experimental data suggested that at the levels predicted over the next century acidification is less of a threat to Caribbean corals compared to warming but that there is evidence for variation across the region and considerable data gaps [89]. Despite this finding, the evidence presented in this paper suggests acidification resilient Caribbean corals maintain increasingly large proton differentials with seawater under acidification, highlighting that there may be an energetic cost to this adaptation that corals would have to maintain indefinitely in the future. The work here also highlights that warming can have complex influences on the calcification processes even outside a severe bleaching event through changes to the partitioning of carbon between the host, symbiont, and the pool of ions used for calcification. The sustainability of these adaptations to acidification and warming are largely unexplored in Caribbean corals, but is highly relevant given findings from this experiment that even if positive net calcification is maintained in environmental challenge experiments corals could be depleting energy reserves [39]. Therefore, it will be important for future research to attempt to determine whether even the relatively resilient species such as *S. siderea* can maintain their short-term adaptive responses over the longer term.

Overall, the results presented here and in previous work on these corals [7,38,39,87] highlight the considerable complexity in host and symbiont responses to ocean warming and acidification, and demonstrate that these responses are closely coupled to a coral's physicochemical control of their calcification process.

Supplementary Materials: The following supporting information can be downloaded at: <https://www.mdpi.com/article/10.3390/jmse10081075/s1>, Table S1: Measured Culture Conditions in the 8 Experimental Setups from Bove et al., 2019; Table S2: Calculated Culture Conditions in the 8 Experimental Setups from Bove et al., 2019; Table S3: Physiological data of the host and the symbionts originally published in Bove et al. (2021) from the same corals used in this study; Table S4: Boron isotope standard reproducibility; Table S5: Reproducibility of B/Ca analyses of CamWuellestorfi and NEP standards; Table S6: Functions used for data transformations according the method of Tukey et al., 1977; Table S7: Geochemical data and calculated parameters from individual Caribbean coral specimens, of which the average per experimental condition are given in main text Tables 1 and 2; Table S8: Average and individual coral specimen geochemical data and calculations from *Stylophora pistillata*; Table S9: AIC results for Caribbean coral geochemical data as a function of the pH of seawater in the experiment and net calcification as a function of calculated CF parameter data; Table S10: Calculations of pH gradient between seawater and the calcifying fluid; Table S11: ANOVA results for Caribbean coral geochemical and physiological data; Table S12: Compilation of published data used in the main text.

Author Contributions: Conceptualization, R.A.E., K.D.C. and J.B.R.; methodology, R.A.E., S.M., K.D.C. and J.B.R.; formal analysis, C.B.B., L.P.C., S.M., B.A.C., M.G., I.D.C. and R.A.E.; investigation, C.B.B., L.P.C., M.G., I.D.C., K.D.C., R.A.E. and J.B.R.; resources, R.A.E., K.D.C. and J.B.R.; data curation, M.G. and R.A.E.; writing—original draft preparation, R.A.E. and I.D.C.; writing—review and editing, all authors; visualization, M.G., I.D.C. and R.A.E.; supervision, R.A.E., K.D.C. and J.B.R.; project administration, R.A.E., K.D.C. and J.B.R.; funding acquisition, R.A.E., K.D.C. and J.B.R. All authors have read and agreed to the published version of the manuscript.

Funding: RAE and JBR acknowledge support from National Science Foundation grants OCE-1437166 and OCE-1437371. KDC acknowledges support from NSF grant OCE-1459522. RAE, MG, ID, and BA were also supported by the “Laboratoire d’Excellence” LabexMER (ANR-10-LABX-19) Chair to RAE, co-funded by a grant from the French government under the program “Investissements d’Avenir” and MG was supported by an IAGC student grant 2017. RAE acknowledges support from the Pritzker Endowment to UCLA IoES, and JBR acknowledges support from the ZMT and the Hanse-Wissenschaftskolleg Fellowship Program. BA was supported by an NSF GRFP. M.G., I.D., and BA were supported by the Center for Diverse Leadership in Science, funded by NSF, the Packard Foundation, Sloan Foundation, and Silicon Valley Community Foundation.

Data Availability Statement: Data will be archived in the BCO-DMO archive on publication of this article (<https://www.bco-dmo.org/>, accessed on 24 July 2022).

Acknowledgments: We thank Belize Fisheries Department for all associated permits, the Toledo Institute for Development and Environment (TIDE), and the Southern Environmental Association (SEA) for their continued support, as well as Garbutt’s Marine for assistance in the field.

Conflicts of Interest: The authors declare no conflict of interest. The funders had no role in the design of the study; in the collection, analyses, or interpretation of data; in the writing of the manuscript, or in the decision to publish the results.

References

1. Glynn, P.W. Coral reef bleaching in the 1980s and possible connections with global warming. *Trends Ecol. Evol.* **1991**, *6*, 175–179. [[CrossRef](#)]
2. Hughes, T.P.; Kerry, J.T.; Álvarez-Noriega, M.; Álvarez-Romero, J.G.; Anderson, K.D.; Baird, A.H.; Babcock, R.C.; Beger, M.; Bellwood, D.R.; Berkemans, R.; et al. Global warming and recurrent mass bleaching of corals. *Nature* **2017**, *543*, 373–377. [[CrossRef](#)] [[PubMed](#)]
3. Doney, S.C.; Fabry, V.J.; Feely, R.A.; Kleypas, J.A. Ocean Acidification: The Other CO₂ Problem. *Annu. Rev. Mar. Sci.* **2009**, *1*, 169–192. [[CrossRef](#)] [[PubMed](#)]
4. Iglesias-Rodríguez, M.D.; Halloran, P.R.; Rickaby, R.E.M.; Hall, I.R.; Colmenero-Hidalgo, E.; Gittins, J.R.; Green, D.R.H.; Tyrrell, T.; Gibbs, S.J.; von Dassow, P.; et al. Phytoplankton Calcification in a High-CO₂ World. *Science* **2008**, *320*, 336–340. [[CrossRef](#)]
5. Ries, J.B.; Cohen, A.L.; McCorkle, D.C. Marine calcifiers exhibit mixed responses to CO₂-induced ocean acidification. *Geology* **2009**, *37*, 1131–1134. [[CrossRef](#)]
6. Kroeker, K.; Micheli, F.; Gambi, M.C. Ocean acidification causes ecosystem shifts via altered competitive interactions. *Nat. Clim. Chang.* **2012**, *3*, 156–159. [[CrossRef](#)]
7. Guillermic, M.; Cameron, L.P.; De Corte, I.; Misra, S.; Bijma, J.; de Beer, D.; Reymond, C.E.; Westphal, H.; Ries, J.B.; Eagle, R.A. Thermal stress reduces pocilloporid coral resilience to ocean acidification by impairing control over calcifying fluid chemistry. *Sci. Adv.* **2021**, *7*, eaba9958. [[CrossRef](#)]
8. Marubini, F.; Atkinson, M. Effects of lowered pH and elevated nitrate on coral calcification. *Mar. Ecol. Prog. Ser.* **1999**, *188*, 117–121. [[CrossRef](#)]
9. Langdon, C.; Takahashi, T.; Sweeney, C.; Chipman, D.; Goddard, J.; Marubini, F.; Aceves, H.; Barnett, H.; Atkinson, M.J. Effect of calcium carbonate saturation state on the calcification rate of an experimental coral reef. *Glob. Biogeochem. Cycles* **2000**, *14*, 639–654. [[CrossRef](#)]
10. Langdon, C. Effect of elevated pCO₂ on photosynthesis and calcification of corals and interactions with seasonal change in temperature/irradiance and nutrient enrichment. *J. Geophys. Res. Earth Surf.* **2005**, *110*, C9. [[CrossRef](#)]
11. Marubini, F.; Barnett, H.; Langdon, C.; Atkinson, M.J. Dependence of calcification on light and carbonate ion concentration for the hermatypic coral *Porites compressa*. *Mar. Ecol. Prog. Ser.* **2001**, *220*, 153–162. [[CrossRef](#)]
12. Renegar, D.; Riegl, B. Effect of nutrient enrichment and elevated CO₂ partial pressure on growth rate of Atlantic scleractinian coral *Acropora cervicornis*. *Mar. Ecol. Prog. Ser.* **2005**, *293*, 69–76. [[CrossRef](#)]
13. Schneider, K.; Erez, J. The effect of carbonate chemistry on calcification and photosynthesis in the hermatypic coral *Acropora eurystroma*. *Limnol. Oceanogr.* **2006**, *51*, 1284–1293. [[CrossRef](#)]
14. Anthony, K.R.N.; Kline, D.I.; Diaz-Pulido, G.; Dove, S.; Hoegh-Guldberg, O. Ocean acidification causes bleaching and productivity loss in coral reef builders. *Proc. Natl. Acad. Sci. USA* **2008**, *105*, 17442–17446. [[CrossRef](#)] [[PubMed](#)]
15. Jokiel, P.L.; Rodgers, K.S.; Kuffner, I.B.; Andersson, A.J.; Cox, E.F.; Mackenzie, F.T. Ocean acidification and calcifying reef organisms: A mesocosm investigation. *Coral Reefs* **2008**, *27*, 473–483. [[CrossRef](#)]
16. Marubini, F.; Ferrier-Pagès, C.; Furla, P.; Allemand, D. Coral calcification responds to seawater acidification: A working hypothesis towards a physiological mechanism. *Coral Reefs* **2008**, *27*, 491–499. [[CrossRef](#)]
17. Krief, S.; Hendy, E.J.; Fine, M.; Yam, R.; Meibom, A.; Foster, G.L.; Shemesh, A. Physiological and isotopic responses of scleractinian corals to ocean acidification. *Geochim. Cosmochim. Acta* **2010**, *74*, 4988–5001. [[CrossRef](#)]

18. Holcomb, M.; Cohen, A.L.; McCorkle, D.C. An investigation of the calcification response of the scleractinian coral *Astrangia poculata* to elevated pCO₂ and the effects of nutrients, zooxanthellae and gender. *Biogeosciences* **2012**, *9*, 29–39. [[CrossRef](#)]
19. Edmunds, P.J.; Brown, D.; Moriarty, V. Interactive effects of ocean acidification and temperature on two scleractinian corals from Moorea, French Polynesia. *Glob. Chang. Biol.* **2012**, *18*, 2173–2183. [[CrossRef](#)]
20. Comeau, S.; Carpenter, R.C.; Edmunds, P.J. Effects of irradiance on the response of the coral *Acropora pulchra* and the calcifying alga *Hydrolithon reinboldii* to temperature elevation and ocean acidification. *J. Exp. Mar. Biol. Ecol.* **2014**, *453*, 28–35. [[CrossRef](#)]
21. Reynaud, S.; Leclercq, N.; Romaine-Lioud, S.; Ferrier-Pagès, C.; Jaubert, J.; Gattuso, J.-P. Interacting effects of CO₂ partial pressure and temperature on photosynthesis and calcification in a scleractinian coral. *Glob. Chang. Biol.* **2003**, *9*, 1660–1668. [[CrossRef](#)]
22. Rodolfo-Metalpa, R.; Martin, S.; Ferrier-Pagès, C.; Gattuso, J.-P. Response of the temperate coral *Cladocora caespitosa* to mid- and long-term exposure to pCO₂ and temperature levels projected for the year 2100 AD. *Biogeosciences* **2010**, *7*, 289–300. [[CrossRef](#)]
23. Edmunds, P.J. Zooplanktivory ameliorates the effects of ocean acidification on the reef coral *Porites* spp. *Limnol. Oceanogr.* **2011**, *56*, 2402–2410. [[CrossRef](#)]
24. Schoepf, V.; Grottooli, A.G.; Warner, M.E.; Cai, W.-J.; Melman, T.F.; Hoadley, K.D.; Pettay, D.T.; Hu, X.; Li, Q.; Xu, H.; et al. Coral Energy Reserves and Calcification in a High-CO₂ World at Two Temperatures. *PLoS ONE* **2013**, *8*, e75049. [[CrossRef](#)] [[PubMed](#)]
25. Cameron, L.P.; Reymond, C.E.; Bijma, J.; Büscher, J.; De Beer, D.; Guillermic, M.; Eagle, R.A.; Gunnell, J.; Müller-Lundin, F.; Schmidt-Greib, G.; et al. Impacts of warming and acidification on coral calcification linked to symbiont loss and deregulation of calcifying fluid pH. *J. Mar. Sci. Eng.* **2022**, unpublished.
26. Innis, T.; Allen-Waller, L.; Brown, K.T.; Sparagon, W.; Carlson, C.; Kruse, E.; Huffmyer, A.S.; Nelson, C.E.; Putnam, H.M.; Barott, K.L. Marine heatwaves depress metabolic activity and impair cellular acid–base homeostasis in reef-building corals regardless of bleaching susceptibility. *Glob. Chang. Biol.* **2021**, *27*, 2728–2743. [[CrossRef](#)]
27. D’Olivo, J.P.; McCulloch, M. Response of coral calcification and calcifying fluid composition to thermally induced bleaching stress. *Sci. Rep.* **2017**, *7*, 2207. [[CrossRef](#)]
28. D’Olivo, J.P.; Ellwood, G.; DeCarlo, T.M.; McCulloch, M. Deconvolving the long-term impacts of ocean acidification and warming on coral biomineralisation. *Earth Planet. Sci. Lett.* **2019**, *526*, 115785. [[CrossRef](#)]
29. Schoepf, V.; D’Olivo, J.P.; Rigal, C.; Jung, E.M.U.; McCulloch, M.T. Heat stress differentially impacts key calcification mechanisms in reef-building corals. *Coral Reefs* **2021**, *40*, 459–471. [[CrossRef](#)]
30. Venn, A.; Tambutté, E.; Holcomb, M.; Allemand, D.; Tambutté, S. Live Tissue Imaging Shows Reef Corals Elevate pH under Their Calcifying Tissue Relative to Seawater. *PLoS ONE* **2011**, *6*, e20013. [[CrossRef](#)]
31. Venn, A.A.; Tambutté, E.; Holcomb, M.; Laurent, J.; Allemand, D.; Tambutté, S. Impact of seawater acidification on pH at the tissue–skeleton interface and calcification in reef corals. *Proc. Natl. Acad. Sci. USA* **2012**, *110*, 1634–1639. [[CrossRef](#)] [[PubMed](#)]
32. Allison, N.; Cohen, I.; Finch, A.A.; Erez, J.; Tudhope, A.W. Corals concentrate dissolved inorganic carbon to facilitate calcification. *Nat. Commun.* **2014**, *5*, 5741. [[CrossRef](#)] [[PubMed](#)]
33. McCulloch, M.T.; D’Olivo, J.P.; Falter, J.; Georgiou, L.; Holcomb, M.; Montagna, P.; Trotter, J.A. Boron Isotopic Systematics in Scleractinian Corals and the Role of pH Up-regulation. In *Boron Isotopes. Advances in Isotope Geochemistry*; Springer: Cham, Switzerland, 2017; pp. 145–162. [[CrossRef](#)]
34. Venn, A.A.; Tambutté, E.; Caminiti-Segonds, N.; Techer, N.; Allemand, D. Effects of light and darkness on pH regulation in three coral species exposed to seawater acidification. *Sci. Rep.* **2019**, *9*, 2201. [[CrossRef](#)] [[PubMed](#)]
35. Sevilgen, D.S.; Venn, A.A.; Hu, M.Y.; Tambutté, E.; de Beer, D.; Planas-Bielsa, V.; Tambutté, S. Full in vivo characterization of carbonate chemistry at the site of calcification in corals. *Sci. Adv.* **2019**, *5*, eaau7447. [[CrossRef](#)]
36. Guo, W. Seawater temperature and buffering capacity modulate coral calcifying pH. *Sci. Rep.* **2019**, *9*, 1189. [[CrossRef](#)] [[PubMed](#)]
37. Chalk, T.B.; Standish, C.D.; D’Angelo, C.; Castillo, K.D.; Milton, J.A.; Foster, G.L. Mapping coral calcification strategies from in situ boron isotope and trace element measurements of the tropical coral *Siderastrea siderea*. *Sci. Rep.* **2021**, *11*, 472. [[CrossRef](#)]
38. Bove, C.B.; Ries, J.B.; Davies, S.W.; Westfield, I.T.; Umbanhowar, J.; Castillo, K.D. Common Caribbean corals exhibit highly variable responses to future acidification and warming. *Proc. R. Soc. B Boil. Sci.* **2019**, *286*, 20182840. [[CrossRef](#)]
39. Bove, C.B.; Davies, S.W.; Ries, J.B.; Umbanhowar, J.; Thomasson, B.C.; Farquhar, E.B.; McCoppin, J.A.; Castillo, K.D. Global change differentially modulates coral physiology and suggests future shifts in Caribbean reef assemblages. *bioRxiv* **2021**. [[CrossRef](#)]
40. Castillo, K.D.; Lima, F.P. Comparison of in situ and satellite-derived (MODIS-Aqua/Terra) methods for assessing temperatures on coral reefs. *Limnol. Oceanogr. Methods* **2010**, *8*, 107–117. [[CrossRef](#)]
41. Barker, S.; Greaves, M.; Elderfield, H. A study of cleaning procedures used for foraminiferal Mg/Ca paleothermometry. *Geochem. Geophys. Geosyst.* **2003**, *4*. [[CrossRef](#)]
42. Gaillardet, J.; Lemarchand, D.; Göpel, C.; Manhès, G. Evaporation and Sublimation of Boric Acid: Application for Boron Purification from Organic Rich Solutions. *Geostand. Geoanal. Res.* **2001**, *25*, 67–75. [[CrossRef](#)]
43. Misra, S.; Owen, R.; Kerr, J.; Greaves, M.; Elderfield, H. Determination of δ¹¹B by HR-ICP-MS from mass limited samples: Application to natural carbonates and water samples. *Geochim. Cosmochim. Acta* **2014**, *140*, 531–552. [[CrossRef](#)]
44. Guillermic, M.; Misra, S.; Eagle, R.; Villa, A.; Chang, F.; Tripathi, A. Seawater pH reconstruction using boron isotopes in multiple planktonic foraminifera species with different depth habitats and their potential to constrain pH and pCO₂ gradients. *Biogeosciences* **2020**, *17*, 3487–3510. [[CrossRef](#)]

45. Lloyd, N.S.; Sadekov, A.Y.; Misra, S. Application of 10^{13} ohm Faraday cup current amplifiers for boron isotopic analyses by solution mode and laser ablation multicollector inductively coupled plasma mass spectrometry. *Rapid Commun. Mass Spectrom.* **2017**, *32*, 9–18. [[CrossRef](#)]
46. McCulloch, M.T.; Holcomb, M.; Rankenburg, K.; Trotter, J.A. Rapid, high-precision measurements of boron isotopic compositions in marine carbonates. *Rapid Commun. Mass Spectrom.* **2014**, *28*, 2704–2712. [[CrossRef](#)]
47. Holcomb, M.; Venn, A.A.; Tambutté, E.; Allemand, D.; Trotter, J.; McCulloch, M.; Tambutte, S. Coral calcifying fluid pH dictates response to ocean acidification. *Sci. Rep.* **2014**, *4*, 5207. [[CrossRef](#)] [[PubMed](#)]
48. Sutton, J.N.; Liu, Y.-W.; Ries, J.B.; Guillermic, M.; Ponzevera, E.; Eagle, R.A. $\delta^{11}\text{B}$ as monitor of calcification site pH in divergent marine calcifying organisms. *Biogeosciences* **2018**, *15*, 1447–1467. [[CrossRef](#)]
49. Gutjahr, M.; Bordier, L.; Douville, E.; Farmer, J.; Foster, G.L.; Hathorne, E.C.; Hönisch, B.; Lemarchand, D.; Louvat, P.; McCulloch, M.; et al. Sub-Permil Interlaboratory Consistency for Solution-Based Boron Isotope Analyses on Marine Carbonates. *Geostand. Geoanal. Res.* **2021**, *45*, 59–75. [[CrossRef](#)]
50. Hemming, N.; Hanson, G. Boron isotopic composition and concentration in modern marine carbonates. *Geochim. Cosmochim. Acta* **1992**, *56*, 537–543. [[CrossRef](#)]
51. Decarlo, T.M.; Comeau, S.; Cornwall, C.E.; McCulloch, M.T. Coral resistance to ocean acidification linked to increased calcium at the site of calcification. *Proc. R. Soc. B Boil. Sci.* **2018**, *285*, 20180564. [[CrossRef](#)]
52. Foster, G.L.; von Strandmann, P.P.; Rae, J. Boron and magnesium isotopic composition of seawater. *Geochem. Geophys. Geosyst.* **2010**, *11*. [[CrossRef](#)]
53. Dickson, A.G. Thermodynamics of the dissociation of boric acid in synthetic seawater from 273.15 to 318.15 K. *Deep Sea Res. Part A Oceanogr. Res. Pap.* **1990**, *37*, 755–766. [[CrossRef](#)]
54. Lee, K.; Kim, T.-W.; Byrne, R.H.; Millero, F.J.; Feely, R.A.; Liu, Y.-M. The universal ratio of boron to chlorinity for the North Pacific and North Atlantic oceans. *Geochim. Cosmochim. Acta* **2010**, *74*, 1801–1811. [[CrossRef](#)]
55. Upadhyay, D.; Lucarelli, J.; Arnold, A.; Flores, R.; Bricker, H.; Ulrich, R.N.; Jesmok, G.; Santi, L.; Defliese, W.; Eagle, R.A.; et al. Carbonate clumped isotope analysis (Δ_{47}) of 21 carbonate standards determined via gas-source isotope-ratio mass spectrometry on four instrumental configurations using carbonate-based standardization and multiyear data sets. *Rapid Commun. Mass Spectrom.* **2021**, *35*, e9143. [[CrossRef](#)] [[PubMed](#)]
56. Tukey, J. *Exploratory Data Analysis*; Addison-Wesley: Reading, MA, USA, 1977.
57. Hönisch, B.; Hemming, N.; Grottoli, A.; Amat, A.; Hanson, G.; Bijma, J. Assessing scleractinian corals as recorders for paleo-pH: Empirical calibration and vital effects. *Geochim. Cosmochim. Acta* **2004**, *68*, 3675–3685. [[CrossRef](#)]
58. Reynaud, S.; Hemming, N.G.; Juillet-Leclerc, A.; Gattuso, J.-P. Effect of pCO₂ and temperature on the boron isotopic composition of the zooxanthellate coral *Acropora* sp. *Coral Reefs* **2004**, *23*, 539–546. [[CrossRef](#)]
59. Trotter, J.; Montagna, P.; McCulloch, M.; Silenzi, S.; Reynaud, S.; Mortimer, G.; Martin, S.; Ferrier-Pagès, C.; Gattuso, J.-P.; Rodolfo-Metalpa, R. Quantifying the pH ‘vital effect’ in the temperate zooxanthellate coral *Cladocora caespitosa*: Validation of the boron seawater pH proxy. *Earth Planet. Sci. Lett.* **2011**, *303*, 163–173. [[CrossRef](#)]
60. Rollion-Bard, C.; Blamart, D.; Trebosc, J.; Tricot, G.; Mussi, A.; Cuif, J.-P. Boron isotopes as pH proxy: A new look at boron speciation in deep-sea corals using ^{11}B MAS NMR and EELS. *Geochim. Cosmochim. Acta* **2011**, *75*, 1003–1012. [[CrossRef](#)]
61. Ries, J.B. A physicochemical framework for interpreting the biological calcification response to CO₂-induced ocean acidification. *Geochim. Cosmochim. Acta* **2011**, *75*, 4053–4064. [[CrossRef](#)]
62. Anagnostou, E.; Huang, K.-F.; You, C.-F.; Sikes, E.; Sherrell, R. Evaluation of boron isotope ratio as a pH proxy in the deep sea coral *Dendrophyllum dianthus*: Evidence of physiological pH adjustment. *Earth Planet. Sci. Lett.* **2012**, *349–350*, 251–260. [[CrossRef](#)]
63. McCulloch, M.; Falter, J.; Trotter, J.; Montagna, P. Coral resilience to ocean acidification and global warming through pH up-regulation. *Nat. Clim. Chang.* **2012**, *2*, 623–627. [[CrossRef](#)]
64. Tanaka, K.; Holcomb, M.; Takahashi, A.; Kurihara, H.; Asami, R.; Shinjo, R.; Sowa, K.; Rankenburg, K.; Watanabe, T.; McCulloch, M. Response of *Acropora digitifera* to ocean acidification: Constraints from $\delta^{11}\text{B}$, Sr, Mg, and Ba compositions of aragonitic skeletons cultured under variable seawater pH. *Coral Reefs* **2015**, *34*, 1139–1149. [[CrossRef](#)]
65. Georgiou, L.; Falter, J.; Trotter, J.; Kline, D.I.; Holcomb, M.; Dove, S.G.; Hoegh-Guldberg, O.; McCulloch, M. pH homeostasis during coral calcification in a free ocean CO₂ enrichment (FOCE) experiment, Heron Island reef flat, Great Barrier Reef. *Proc. Natl. Acad. Sci. USA* **2015**, *112*, 13219–13224. [[CrossRef](#)]
66. Cai, W.J.; Ma, Y.; Hopkinson, B.M.; Grottoli, A.G.; Warner, M.E.; Ding, Q.; Hu, X.; Yuan, X.; Schoepf, V.; Xu, H.; et al. Microelectrode characterization of coral daytime interior pH and carbonate chemistry. *Nat. Commun.* **2016**, *7*, 11144. [[CrossRef](#)]
67. Comeau, S.; Cornwall, C.E.; McCulloch, M. Decoupling between the response of coral calcifying fluid pH and calcification to ocean acidification. *Sci. Rep.* **2017**, *7*, 7573. [[CrossRef](#)]
68. Comeau, S.; Tambutté, E.; Carpenter, R.C.; Edmunds, P.J.; Evensen, N.R.; Allemand, D.; Ferrier-Pagès, C.; Venn, A.A. Coral calcifying fluid pH is modulated by seawater carbonate chemistry not solely seawater pH. *Proc. R. Soc. B Boil. Sci.* **2017**, *284*, 20161669. [[CrossRef](#)] [[PubMed](#)]
69. Liu, Y.-W.; Sutton, J.N.; Ries, J.B.; Eagle, R.A. Regulation of calcification site pH is a polyphyletic but not always governing response to ocean acidification. *Sci. Adv.* **2020**, *6*, eaax1314. [[CrossRef](#)]

70. Allison, N.; Cole, C.; Hintz, C.; Hintz, K.; Rae, J.; Finch, A. Resolving the interactions of ocean acidification and temperature on coral calcification media pH. *Coral Reefs* **2021**, *40*, 1807–1818. [[CrossRef](#)]
71. Allison, N.; Cohen, I.; Finch, A.A.; Erez, J. Controls on Sr/Ca and Mg/Ca in scleractinian corals: The effects of Ca-ATPase and transcellular Ca channels on skeletal chemistry. *Geochim. Cosmochim. Acta* **2011**, *75*, 6350–6360. [[CrossRef](#)]
72. Pierrot, D.; Lewis, E.; Wallace, D.W.R. MS Excel Program Developed for CO₂ System Calculations. In *Carbon Dioxide Information Analysis Center, Oak Ridge National Laboratory*; U.S. Department of Energy: Oak Ridge, TN, USA, 2006. [[CrossRef](#)]
73. Al-Horani, F.A.; Almoghrabi, S.M.; De Beer, D. The mechanism of calcification and its relation to photosynthesis and respiration in the scleractinian coral *Galaxea fascicularis*. *Mar. Biol.* **2003**, *142*, 419–426. [[CrossRef](#)]
74. McCulloch, M.T.; D’Olivo, J.P.; Falter, J.; Holcomb, M.; Trotter, J. Coral calcification in a changing World and the interactive dynamics of pH and DIC upregulation. *Nat. Commun.* **2017**, *8*, 15686. [[CrossRef](#)] [[PubMed](#)]
75. Allison, N. Reconstructing coral calcification fluid dissolved inorganic carbon chemistry from skeletal boron: An exploration of potential controls on coral aragonite B/Ca. *Heliyon* **2017**, *3*, e00387. [[CrossRef](#)] [[PubMed](#)]
76. Mavromatis, V.; Montouillout, V.; Noireaux, J.; Gaillardet, J.; Schott, J. Characterization of boron incorporation and speciation in calcite and aragonite from co-precipitation experiments under controlled pH, temperature and precipitation rate. *Geochim. Cosmochim. Acta* **2015**, *150*, 299–313. [[CrossRef](#)]
77. Holcomb, M.; DeCarlo, T.; Gaetani, G.; McCulloch, M. Factors affecting B/Ca ratios in synthetic aragonite. *Chem. Geol.* **2016**, *437*, 67–76. [[CrossRef](#)]
78. Mass, T.; Giuffre, A.J.; Sun, C.-Y.; Stifler, C.A.; Frazier, M.J.; Neder, M.; Tamura, N.; Stan, C.V.; Marcus, M.A.; Gilbert, P.U.P.A. Amorphous calcium carbonate particles form coral skeletons. *Proc. Natl. Acad. Sci. USA* **2017**, *114*, E7670–E7678. [[CrossRef](#)]
79. Evans, D.; Gray, W.R.; Rae, J.; Greenop, R.; Webb, P.B.; Penkman, K.; Kröger, R.; Allison, N. Trace and major element incorporation into amorphous calcium carbonate (ACC) precipitated from seawater. *Geochim. Cosmochim. Acta* **2020**, *290*, 293–311. [[CrossRef](#)]
80. Ulrich, R.N.; Guillermic, M.; Campbell, J.; Hakim, A.; Han, R.; Singh, S.; Stewart, J.D.; Román-Palacios, C.; Carroll, H.M.; De Corte, I.; et al. Patterns of Element Incorporation in Calcium Carbonate Biominerals Recapitulate Phylogeny for a Diverse Range of Marine Calcifiers. *Front. Earth Sci.* **2021**, *9*, 641760. [[CrossRef](#)]
81. Giuffre, A.J.; Gagnon, A.C.; De Yoreo, J.J.; Dove, P.M. Isotopic tracer evidence for the amorphous calcium carbonate to calcite transformation by dissolution–reprecipitation. *Geochim. Cosmochim. Acta* **2015**, *165*, 407–417. [[CrossRef](#)]
82. Von Euw, S.; Zhang, Q.; Manichev, V.; Murali, N.; Gross, J.; Feldman, L.C.; Gustafsson, T.; Flach, C.; Mendelsohn, R.; Falkowski, P.G. Biological control of aragonite formation in stony corals. *Science* **2017**, *356*, 933–938. [[CrossRef](#)]
83. Swart, P.; Leder, J.; Szmant, A.; Dodge, R. The origin of variations in the isotopic record of scleractinian corals: II. Carbon. *Geochim. Cosmochim. Acta* **1996**, *60*, 2871–28856. [[CrossRef](#)]
84. Grottoli, A.G. Effect of light and brine shrimp on skeletal $\delta^{13}\text{C}$ in the Hawaiian coral *Porites compressa*: A tank experiment. *Geochim. Cosmochim. Acta* **2002**, *66*, 1955–1967. [[CrossRef](#)]
85. Baker, A.C. Reef corals bleach to survive change. *Nature* **2001**, *411*, 765–766. [[CrossRef](#)] [[PubMed](#)]
86. Baker, D.M.; Freeman, C.J.; Wong, J.C.; Fogel, M.L.; Knowlton, N. Climate change promotes parasitism in a coral symbiosis. *ISME J.* **2018**, *12*, 921–930. [[CrossRef](#)] [[PubMed](#)]
87. Castillo, K.D.; Ries, J.B.; Bruno, J.F.; Westfield, I.T. The reef-building coral *Siderastrea siderea* exhibits parabolic responses to ocean acidification and warming. *Proc. R. Soc. B Boil. Sci.* **2014**, *281*, 20141856. [[CrossRef](#)] [[PubMed](#)]
88. Okazaki, R.R.; Towle, E.K.; Hooidonk, R.; Mor, C.; Winter, R.N.; Piggot, A.M.; Cuning, R.; Baker, A.; Klaus, J.S.; Swart, P.K.; et al. Species-specific responses to climate change and community composition determine future calcification rates of Florida Keys reefs. *Glob. Chang. Biol.* **2016**, *23*, 1023–1035. [[CrossRef](#)]
89. Bove, C.B.; Umbanhowar, J.; Castillo, K.D. Meta-Analysis Reveals Reduced Coral Calcification Under Projected Ocean Warming but Not Under Acidification Across the Caribbean Sea. *Front. Mar. Sci.* **2020**, *7*, 127. [[CrossRef](#)]